Zhuang *et al*. *Mil Med Res* 2026
https://doi.org/10.1016/j.mmr.2026.100003

MMR MILITARY MEDICAL RESEARCH

RESEARCH Open Access

tDCS improves early Alzheimer's disease by synaptic vesicle fusion and release

Yue-Yang Zhuang[1†], Jia-Min Yan[1†], Tie-Cheng Wu[1,2†], Wen-Shan Xu[1], Bao Wu[1], Xi Xie[1], Wen-Ju Wang[1], Hua-Wei Lin[1], Jia-Wei Jian[1], Jun-Zi Wang[1], Tao Jiang[1], Li-Ming Chen[1], Yu-Xi Qiu[1], Zhong-Yi Hu[1], Yi-Hui Zhou[1], Ting Yang[1], Min-Guang Yang[1,2], Jing-Fang Zhu[1,2], Jing Tao[1,2], Li-Dian Chen[1,2], Wei-Guang Li[3,4*], Kai Yan[5*] and Wei-Lin Liu[1,2*]

Abstract

Background: Working memory deficits, one of the earliest hallmarks of Alzheimer's disease (AD), are closely linked to abnormal neural activity in the dorsolateral prefrontal cortex (DLPFC). Transcranial direct current stimulation (tDCS), a non-invasive neuromodulation therapy, has been shown to ameliorate early AD working memory deficits by modulating excitatory activity in the DLPFC, yet the underlying mechanisms remain incompletely understood.

Methods: This investigation was structured around three experimental phases. We initially applied tDCS to stimulate the left prefrontal cortex (PFC) of transgenic mice with 5 familial AD (5×FAD) 5 d per week for 4 weeks. Subsequently, we employed optogenetic (Opt) techniques to modulate left PFC glutamatergic neurons. Finally, we inhibited soluble N-ethylmaleimide-sensitive factor attachment receptor (SNARE) expression in the left PFC to elucidate the essential function of SNARE complex assembly with chaperone molecules in orchestrating synaptic vesicle release.

Results: tDCS treatment improved working memory deficits in early-stage AD mice. This was accompanied by increased cerebral blood flow, enhanced neuronal excitability, amelioration of neurochemical metabolic disorders, and reduced amyloid β-protein (Aβ) deposition in the left PFC. Opt stimulation of PFC glutamatergic neurons similarly improved working memory, indicating the association between tDCS's therapeutic effects and synaptic plasticity of excitatory neurons. Crucially, tDCS facilitated synaptic vesicle fusion and release, evidenced by increased vesicle numbers, enhanced release probability, improved synaptic transmission efficacy, and upregulation of the SNARE complex, Snap25, and Syt1. Inhibiting SNARE expression in the left PFC attenuated the tDCS-induced improvements in synaptic vesicle release and working memory.

Conclusion: These findings collectively demonstrate that left PFC-targeted tDCS modulates interactions between the SNARE complex and chaperone molecules, thereby promoting synaptic vesicle fusion and release. This mechanism underlies the amelioration of early AD-like working memory impairment by tDCS.

Key words Transcranial direct current stimulation (tDCS), Dorsolateral prefrontal cortex (DLPFC), Glutamatergic neurons, Synaptic vesicle transport, Working memory

Background

Alzheimer's disease (AD), a progressive neurodegenerative disorder, constitutes the leading cause of dementia worldwide. Currently accounting for over 50% of all dementia cases, its prevalence is projected to rise to 152.8 million cases by 2050 [1]. Among the spectrum of clinical manifestations in AD, working memory impairment represents a core feature that significantly compromises daily functioning. This impairment manifests as difficulties navigating familiar environments and recalling personal belongings [2]. While pharmacological interventions for AD, such as Aducanumab, Donepezil, Galantamine, Rivastigmine, and Memantine, are available, they are frequently associated with adverse effects ranging from nausea and vomiting to bradycardia and seizures [3]. Given the adverse effects associated with these pharmacological treatments, non-pharmacotherapeutic approaches have attracted increasing attention.

In recent years, various neuromodulation techniques, including transcranial direct current stimulation (tDCS), optogenetics (Opt), and transcranial magnetic stimulation, have emerged as promising non-pharmacotherapeutic interventions for cognitive rehabilitation research [4]. Among these, tDCS,

†Yue-Yang Zhuang, Jia-Min Yan, and Tie-Cheng Wu contributed equally to this work.
*Correspondence: Wei-Guang Li, wgli@icmm.ac.cn; Kai Yan, fhyankai@gmail.com; Wei-Lin Liu, liuweilin12@fjtcm.edu.cn
[1]The Institute of Rehabilitation Industry, Fujian University of Traditional Chinese Medicine, Fuzhou 350122, China
[3]State Key Laboratory for Quality Ensurance and Sustainable Use of Dao-di Herbs, Artemisinin Research Center, and Institute of Chinese Materia Medica, China Academy of Chinese Medical Sciences, Beijing 100700, China
Full list of author information is available at the end of the article

Received: 26 August 2025 Accepted: 05 March 2026

© The Author(s) 2026. **Open Access** This article is licensed under a Creative Commons Attribution 4.0 International License, http://creativecommons.org/licenses/by/4.0/ which permits use, sharing, adaptation, distribution and reproduction in any medium or format, as long as you give appropriate credit to the original author(s) and the source, provide a link to the Creative Commons licence, and indicate if changes were made.

a non-invasive brain stimulation technique, offers several advantages such as minimal invasiveness, low cost, and ease of use [5]. Although Opt is invasive, it is a highly precise modulation technique capable of selectively activating specific cell populations within defined brain regions during cognitive rehabilitation [6]. A meta-analysis concluded that tDCS effectively enhances working memory in patients with mild cognitive impairment and AD, with therapeutic effects lasting up to one month post-intervention [7]. Moreover, an animal study revealed that active tDCS applied to the prefrontal cortex (PFC) improved memory function in AD model mice [8]. Further clinical investigations demonstrate that tDCS targeting the dorsolateral prefrontal cortex (DLPFC) can ameliorate working memory deficits in patients with mild neurocognitive disorder and AD [9,10]. Mechanistically, tDCS modulates neural activity and regulates synaptic plasticity by delivering low-intensity direct currents through anodal and cathodal electrodes placed on the scalp, thereby enhancing or suppressing cortical excitability [11]. An animal research shows that tDCS enhances cortical neuron excitability and particularly enhances motor learning task-relevant regional neural activity, facilitating synaptic transmission [12]. However, the precise neurobiological mechanisms underlying these effects remain incompletely elucidated.

In the PFC, the DLPFC is a core brain area responsible for working memory [13]. By facilitating real-time encoding, maintenance, and manipulation of working memory representations, the DLPFC critically mediates spatial information retention, content manipulation, decision-making processes, memory strategy implementation, and mnemonic organization [14]. Studies indicated that progressive working memory deficits in AD were linked to the amyloid β-protein (Aβ) deposition within the DLPFC [15,16]. Aβ-mediated synaptotoxicity triggers synaptic loss and neuronal death, further exacerbating DLPFC dysfunction [15]. Notably, neuroimaging evidence highlighted the left DLPFC as a critical neural locus for working memory manipulation, showing significantly greater activation in this region during working memory tasks than in the right DLPFC [17]. A clinical study showed that synaptic function within the left DLPFC was closely associated with working memory performance in AD patients [16]. Moreover, targeted activation of the left DLPFC during N-back paradigms enhanced working memory performance in AD patients, with these cognitive improvements exhibiting strong dependence on synaptic efficacy modulation [18]. Consequently, synaptic dysfunction in the left DLPFC is among the most important causes of working memory deficits in AD.

Synapses constitute the fundamental structural and functional units for memory encoding and storage. The maintenance of normal working memory depends on sustained high-frequency neuronal firing and coordinated network oscillations in the PFC-physiological processes that fundamentally rely on efficient synaptic communication [19]. Synaptic vesicle fusion and release critically determine intersynaptic communication [13], with its conceptual framework established by Nobel laureates Thomas Südhof and James Rothman, who elucidated the molecular mechanisms governing vesicle transport and release [20]. Glu, the primary excitatory neurotransmitter in the central nervous system, is loaded into vesicles via the vesicular glutamate transporter 1 (VGLUT1) [21]. Further study has revealed that the soluble N-ethylmaleimide-sensitive factor attachment receptor (SNARE) complex is the core molecular machinery driving glutamate (Glu)-containing synaptic vesicle fusion and release [22]. SNARE complex, in concert with dynamin, guide the precise translocation of vesicles to the presynaptic active zone. At this site, Ca^{2+}-dependent rapid vesicle fusion facilitates Glu release into the synaptic cleft, culminating in glutamatergic vesicle trafficking [23]. Research indicates that the expression levels of synaptic vesicle-associated proteins are directly correlated with excitatory neuronal activity [24]. Notably, targeted augmentation of SNARE complex assembly enhances synaptic vesicle fusion and release probabilities, concomitantly improving working memory [25,26]. Further investigations underscore the critical roles played by SNARE complexes and chaperone molecules in regulating synaptic vesicle fusion and neurotransmitter release [27]. These findings suggest that targeting SNARE complexes and chaperone molecules involved in synaptic vesicle fusion and release may be an effective strategy to ameliorate early working memory deficits in AD.

In the exploration of non-invasive brain stimulation techniques, tDCS has shown potential to promote synaptic vesicle activity [28] and enhance synaptic dynamics in presynaptic membranes [29], thereby improving cognitive performance. Nevertheless, the mechanisms by which tDCS affects SNARE-mediated synaptic vesicle fusion and release remain to be fully assessed and understood. This study aimed to elucidate the impact of tDCS on working memory deficits in early AD and to investigate its effects on SNARE-mediated synaptic vesicle fusion and release. By elucidating the mechanisms through which tDCS modulates presynaptic function, we sought to provide novel evidence for its neurobiological basis in improving cognitive function. These findings may inform the development of tDCS-based therapeutic strategies for early AD.

Materials and methods

Experimental animals and grouping

The transgenic mice with 5 familial AD (5×FAD) were purchased from Qianbi Biotechnology Co., Ltd., and used for breeding. Subsequently, the resulting offspring were screened by PCR genotyping to select the 3.5-month-old 5×FAD male mice. A total of 113 wild-type (WT) mice and 456 5×FAD male mice were used in the experiments. Animals were housed in the SPF-level laboratory at the Experimental Animal Center, Fujian University of Traditional Chinese Medicine [SYXK(Fujian)2020-0002]. Animals were maintained on the 12 h/12 h light-dark cycles, temperature (22±2) °C, and relative humidity (40%–65%) with the chow diet and water available ad libitum. After genotypic confirmation of 5×FAD positivity, each mouse was ear-tagged for identification and group assignment. A completely randomized grouping method was used to assign mice to experimental groups. Specifically, all eligible mice were assigned a number, and a computer-generated random number table was applied to ensure equal probability of assignment to each group, thereby minimizing selection bias. For more detailed information on the experimental design, please refer to Additional file 1: Materials and methods. All the experimental procedures in mice were performed in compliance with the protocol approved by the Animal Experiment Ethics Committee of Fujian University of Traditional Chinese Medicine (FJTCMIACUC2023131) and the Animal Research: Reporting *in vivo* Experiments (ARRIVE) guidelines.

tDCS treatment

In the first part, the tDCS group mice received anodic tDCS stimulation while the Sham-tDCS group received anodic sham stimulation. In the third part, the tDCS group, tDCS+tettoxlc group, and tDCS+enhanced green fluorescent protein (EGFP) group mice were treated with anodic tDCS stimulation. The anodic electrode stimulation site was the left PFC, and the cathodic electrode was placed on the thoracic abdomen of the mice. Using the tDCS device, Sham-tDCS stimulation mode, the set current was 250 μA for 20 min. The Sham-tDCS stimulation was likewise applied 5 d per week for 4 consecutive weeks. As described previously [30], the tDCS stimulation current intensity was 250 μA for 20 min, and the intervention was performed 5 d per week for 4 weeks. Wild and 5×FAD group mice were captured under equivalent conditions but not given any treatment. Detailed stimulation parameters and tDCS device settings are provided in Additional file 1: Materials and methods.

Opt stimulation paradigm

An integrated Opt approach was employed for circuit-specific manipulation. Following injection of 200 nl of rAAV-CaMKIIa-hChR2(H134R)-mCherry-WPRE-hGH polyA (AAV2/5 serotype; supplied by BrainTVA Co., Ltd., Wuhan, China) into the left PFC of mice in the Opt and Sham-Opt groups, fiber optic catheters were implanted. Detailed injection and installation procedures are provided in Additional file 1: Materials and methods. After three weeks for adeno-associated virus (AAV) expression, mice were connected to the RWD IOS-465 intelligent Opt system (RWD Life Science Co., Ltd., Shenzhen, China) for daily stimulation sessions (5 min/d for one week). The Opt group received 473 nm light (10 Hz, 3 ms pulses, 1 mW), while the Sham-Opt group received 589 nm light with identical parameters as the Opt group [31]. All procedures were performed aseptically.

Functional ultrasound (FUS) imaging

Functional ultrasonography was used to detect the effect of tDCS stimulation on the activity of left PFC brain regions. Three mice were randomly selected from each of the tDCS group and the Sham-tDCS group. After anesthesia with 2% isoflurane, the mice were fixed on a brain stereotactic device, the hair was removed, and the skull was exposed. The gel was evenly applied to the surface of the skull, and FUS scanning was started for a total of 10 min, with no stimulation during the first 5 min, which was recorded as the baseline level. After that, we applied the stimulation to observe changes in cerebral blood volume (CBV) in the left PFC, which could reflect changes in brain area activity.

Electroencephalogram (EEG)

EEG activity from awake mice in the cage was recorded for 10 min. Finally, the collected EEG data were analyzed using the NeuroExplorer system (Nex Technologies, USA), and depressive filtering was employed to eliminate the influence of alternating current and the relative power $[P_{XX}(f)=(1/(F_S \cdot N))\times|X(f)|^2]$ of the 0–48 Hz alternating current. Delta, theta, alpha, beta, low gamma, and high gamma spectra were compared (percentage of the total number from 0–48 Hz). $X(f)$ is the Fourier transform of the signal $x(n)$, where F_S is the sampling frequency, and N is the signal length. These were summed and defined as delta wave amplitude, theta wave amplitude, alpha wave amplitude, beta wave amplitude, low gamma wave amplitude, and high gamma wave amplitude, denoting delta activity, theta activity, alpha activity, beta activity, low gamma activity, and high gamma activity, respectively. The method for installing EEG electrodes is

described in Additional file 1: Materials and methods.

Whole-brain c-Fos tissue transparent three-dimensional (3D) imaging

We probed brain regions responsive to tDCS stimulation using whole-brain c-Fos tissue-transparent 3D imaging.

Mouse tail intravenous injection

Mice were first subjected to tail vein injection of rAAV-PHP.eB-cFos-EYFP virus, the dose of virus injected was consistent with previously published literature [32]. The injection dose was 1×10^{11} viral genomes per mouse [in 100 μl phosphate-buffered saline (PBS)], using a viral titer of 3.89×10^{12} vg/ml. It took three weeks for the virus to stabilize its expression, so anodic tDCS intervention was performed 4 weeks after injection.

Tissue transparency and 3D imaging

After the tDCS intervention, mice were perfused with 0.01 mol/L PBS and 4% paraformaldehyde, and brain tissues were removed and post-fixed in 4% paraformaldehyde for 24 h. Subsequently, agarose powder and distilled water were prepared to make a 3%–5% mixture solution. The post-fixed mouse brains were embedded in the agarose solution until solidification. Subsequently, the embedded blocks were fixed on a sample holder with glue, and 3D whole-body imaging was performed using a Bio-Mapping 9000 system with a tomographic imaging strategy and a thickness of 40 μm per image. Imaging conditions: Magnification 4×, dual-side illumination, excitation channel 488 nm. Imaging resolution: X, 3.3 μm; Y, 3.3 μm; Z, 7 μm.

Transmission electron microscopy (TEM)

A TEM (Hitachi, Japan) was used to observe the synaptic vesicle in the left PFC. The preparation process for brain slices used in electron microscopy is detailed in Additional file 1: Materials and methods. Synapses with round vesicles, asymmetric synapses, and a single large synaptic contact were presumed to be an excitatory synapse. We calculated the total number of synaptic vesicles in the presumable excitatory synapses and then averaged the number to obtain the number/synapse. For unbiased quantitative analysis, electron microscope images were acquired using systematic random sampling from each experimental group. All images were assigned coded identifiers and analyzed by an investigator blinded to the experimental conditions. This blinding protocol was maintained throughout image processing and data quantification to prevent observational bias.

Electrophysiology

The mice were anesthetized and immediately decapitated, and the intact brain tissue was removed. The brain tissue was trimmed with a surgical blade to preserve the brain tissue containing the left PFC region. This specific brain tissue was then rapidly and stably fixed in a sectioning tank containing 200 ml of pre-oxygenated (95% O_2+5% CO_2 gas mixture) cerebrospinal fluid. Brain slices with a thickness of 400 μm were cut and subsequently incubated in a thermostatic bath at 30 °C and in room-temperature water to fully restore and stabilize the slices' functional state. Membrane-clamp electrophysiological assays were performed on the completed incubated brain slices to probe the electrophysiological properties of neurons in the left PFC region. For more detailed operating steps, please refer to Additional file 1: Materials and methods.

Fiber photometry

Inject rAAV-hSyn-GCaMP6s-WPRE-hGH pA (serotype AAV2/9; titer: 5.83×10^{12} vg/ml; supplied by BrainTVA Co., Ltd., Wuhan, China) into the left PFC and implant the ceramic ferrule integrated with an optical fiber. Signals were recorded three weeks after virus injection. Calcium signals were acquired using RWD Life Science's multi-channel fiber photometry system (RWD Life Science Co., Ltd., Shenzhen, China), synchronized with behavioral video recording (RWD Life Science's camera) during the novel object recognition test (NOR) task. For a more detailed trial protocol and analysis procedure, please refer to Additional file 1: Materials and methods.

Magnetic resonance spectroscopy scanning (MRS)

Hydrogen proton magnetic resonance spectroscopy (^{1}H-MRS) was applied to analyze the levels of Glu, N-acetylaspartate (NAA), and choline (Cho) in the left PFC. A 9.4 T small animal MRI scanner (94/30 USR, Bruker Biopin GMbls, Germany) was used for T2-weighted image (T2WI) and ^{1}H-MRS scan. Mice were anesthetized with 1.5% isoflurane and placed on the scanning bed in the prone position. During the scan, water-circulation heating was used to maintain temperature, and respiration was detected at all times. The specific scanning parameters of T2WI were as follows: repetition time (TR)=2500 ms, echo time (TE)=33 ms, Averages=2, Repetitions=1, Slice thickness=0.7 mm, Slice=15, Image size=256×256, Field of view (FOV)=20 mm×20 mm. For a more detailed analysis procedure, please refer to Additional file 1: Materials and methods.

Blinding procedures

Throughout the intervention (e.g., behavioral tests) and outcome assessment (e.g., histological analysis, statistical evaluation), experimenters remained blinded to group assignments. An independent researcher not involved in the study performed the coding, and group identities were revealed only after data analysis was completed.

Statistical analysis

Statistical analyses were performed using SPSS 28.0, and data visualization was conducted in GraphPad Prism 8.01. We assessed data normality using the Shapiro-Wilk test. For non-normal distributions, we applied Blom's rank-based inverse normal transformation, with persistent non-normal data analyzed using the Kruskal-Wallis test. Normally distributed data are presented as mean±standard deviation (SD), while non-normal data are expressed as median (interquartile range). We employed one-way ANOVA for data with homogeneous variances and Welch's ANOVA for data with heterogeneous variances to examine group differences. This analytical framework was applied to the following comparisons: WT vs. 5×FAD vs. Sham-tDCS vs. tDCS; WT vs. 5×FAD vs. Sham-Opt vs. Opt; and tDCS vs. tDCS+EGFP vs. tDCS+tettoxlc. For ΔCBV comparisons specifically between tDCS and Sham-tDCS groups, we used independent *t*-tests; otherwise, the Mann-Whitney *U* test was applied.

Following significant main effects, we conducted appropriate post-hoc analyses: Bonferroni tests for normally distributed data with homogeneous variances, Games-Howell tests for normally distributed data with heterogeneous variances, and Bonferroni-adjusted post-hoc tests following Kruskal-Wallis analysis for non-normal data. A significance threshold of $P<0.05$ was applied throughout all analyses.

Results

tDCS improved working memory in 5×FAD mice

To better model AD pathology, we utilized 5×FAD mice. To accurately depict our methodology, Fig. 1a presents the tDCS intervention protocol, while Fig. 1b illustrates the experimental flowchart.

Working memory function in each group was assessed before and after the tDCS intervention using spontaneous alternation behavior in the Y-maze test (Fig. 1c). Pre-intervention results revealed a significantly lower spontaneous alternation rate in the 5×FAD group than in the WT group. No statistical differences emerged among the 5×FAD, Sham-tDCS, and tDCS groups, indicating working memory deficits in 3.5-month-old 5×FAD mice and equivalent baseline working memory levels across these groups (Fig. 1d). Post-tDCS intervention, the Y-maze test demonstrated a significantly decreased spontaneous alternation rate in the 5×FAD group vs. the WT group. Conversely, the tDCS group exhibited a significantly higher rate than both the 5×FAD and Sham-tDCS groups, while no significant difference existed between the Sham-tDCS and 5×FAD groups (Fig. 1d). NOR indicated an increased discrimination index in the tDCS group relative to the the 5×FAD and Sham-tDCS groups (Fig. 1e). Furthermore, morris water maze (MWM) data (days 1–5) showed the ratio of second to first escape latency was significantly lower in the tDCS group than both the 5×FAD and Sham-tDCS groups. The average latency ratio across the 5 d also decreased in the tDCS group. No statistically significant difference emerged between the Sham-tDCS and 5×FAD groups (Fig. 1f). These findings demonstrate that tDCS effectively improves working memory function in 5×FAD mice.

tDCS activated the left PFC in 5×FAD mice

To examine whether tDCS intervention activates neurons in the left PFC of 5×FAD mice, we employed whole-brain c-Fos tissue-clearing and 3D imaging. Compared with the Sham-tDCS group, the tDCS group showed a clear enhancement of c-Fos positive signals in the left PFC, indicating that tDCS promotes neuronal activation in this region (Fig. 2a). Given that no activation trend was detected in the right PFC between the tDCS and Sham-tDCS groups, subsequent quantitative immunofluorescence analysis was focused on the left PFC. Immunofluorescence analysis revealed a statistically significant reduction in c-Fos positive cells within the left PFC of 5×FAD mice relative to the WT group. Conversely, the tDCS group showed significantly higher c-Fos positive cell counts than both the 5×FAD and Sham-tDCS groups. No statistically significant difference emerged between the Sham-tDCS and 5×FAD groups (Fig. 2b). Furthermore, to assess the effect of tDCS on the activation of the left PFC brain region in 5×FAD mice, we utilized FUS to record CBV in the left PFC brain region before and after the tDCS intervention. FUS was performed for a total of 10 min, and the first 5 min were recorded as the baseline level. At the 300th second stimulation, the tDCS stimulation was given (or the Sham-tDCS stimulation), and the second 5 min were recorded as the change in CBV during the intervention period. The FUS results observed a significant increase in CBV in the tDCS group during the second 5 min compared to the Sham-tDCS group (Fig. 2c), indicating that the cerebral blood flow in the left PFC was significantly increased after tDCS intervention. In the chronological CBV sequence plot, the relative Doppler values of the left PFC brain

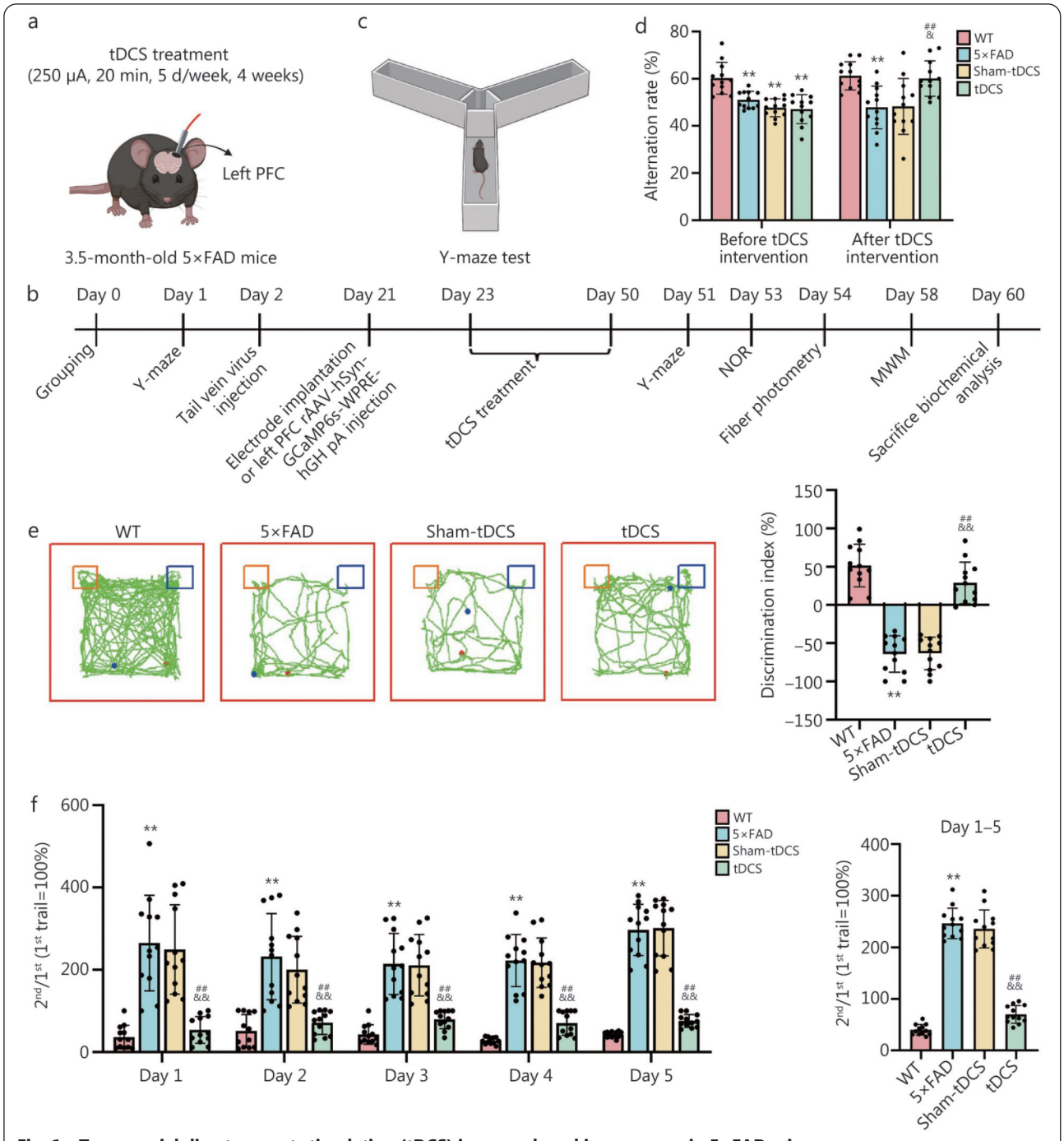

Fig. 1 Transcranial direct current stimulation (tDCS) improved working memory in 5×FAD mice.
a The diagram of the tDCS intervention mode. **b** Schedule of in 5×FAD mice. **c** Schematic diagram of the Y-maze spontaneous alternate test. **d** Spontaneous alternation rate of Y-maze before tDCS intervention (n=12) and after tDCS intervention (n=12). **e** Trajectory diagram and discrimination index for novel object recognition test (NOR) after tDCS intervention (n=12). **f** The ratio of the second time to the first time of the working memory morris water maze (MWM) avoidance latency period after tDCS intervention (n=12). All data are expressed as mean±SD. One-way analysis of variance and Kruskal-Wallis test, $^{**}P$<0.01 vs. WT group; $^{\#\#}P$<0.01 vs. 5×FAD group; $^{\&}P$<0.05, $^{\&\&}P$<0.01 vs. Sham-tDCS group. WT. Wild-type; 5×FAD. Transgenic mice with 5 familial AD

region in the tDCS group were significantly enhanced from baseline after the 300th second stimulation (Fig. 2d), showing that tDCS significantly activated the left PFC brain region. On the contrary, there was no difference in the relative Doppler values of the left PFC brain region of mice in the Sham-tDCS group from the baseline level after the 300th second stimulation, revealing that the Sham-tDCS group did not activate the left PFC brain region.

We monitored EEG activity in the left PFC region of 5×FAD mice using wireless EEG equipment (Fig. 2e-f). By analyzing the relative power of each EEG band (as a percentage of the total number of 0–48 Hz), it was found that there was no significant difference between the groups in all frequency bands after tDCS intervention (Fig. 2e-f).

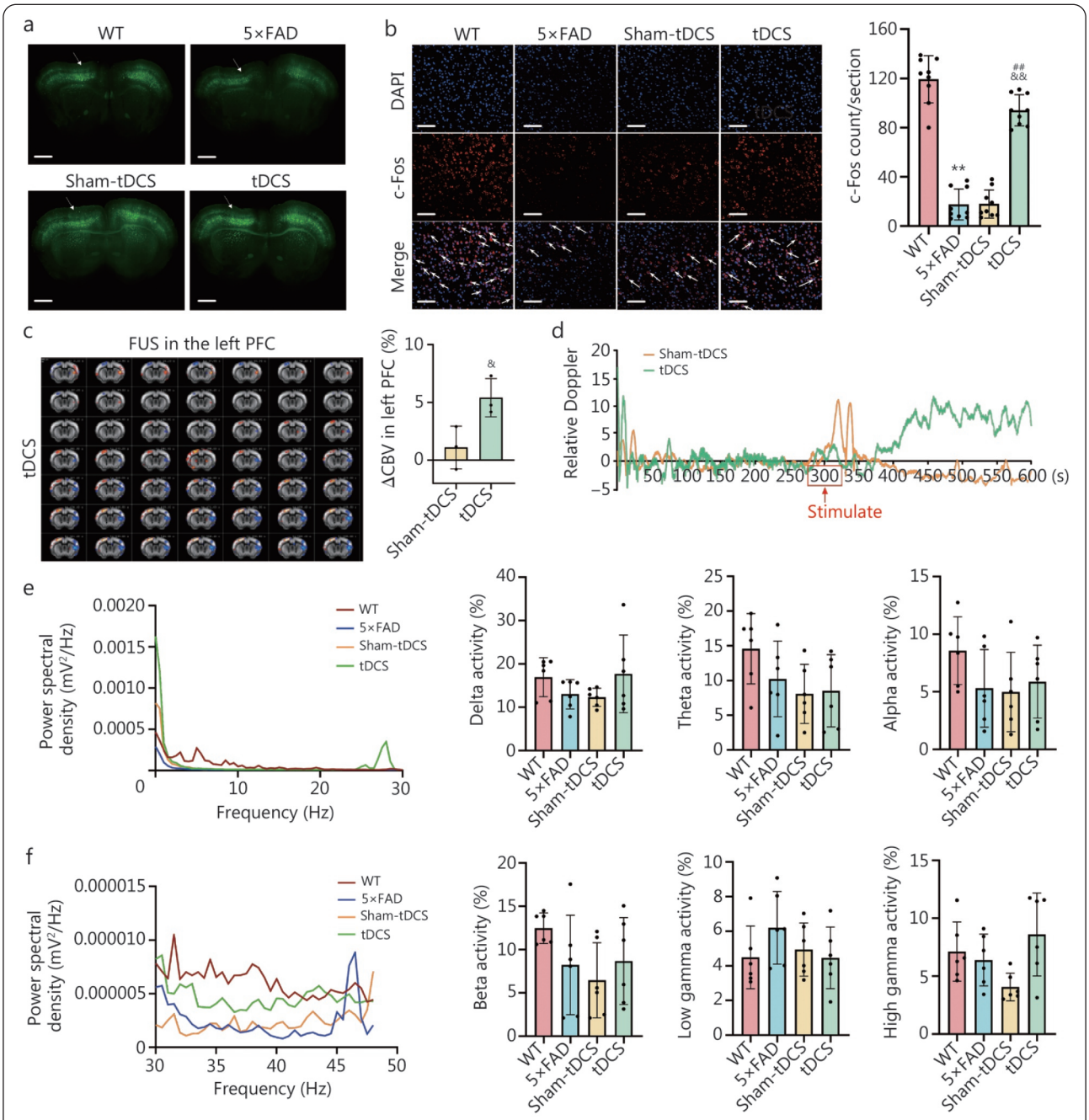

Fig. 2 Transcranial direct current stimulation (tDCS) activated the left prefrontal cortex (PFC) in 5×FAD mice.
a c-Fos imaging results of whole brain showed positive neurons in anterior and posterior prefrontal lobes after tDCS intervention (n=3). White arrows indicate neuronal c-Fos positive signals within the left PFC. Scale bar=500 μm. **b** Immunofluorescence (IF) staining of c-Fos positive cell counts in left PFC after tDCS intervention (n=9). Scale bar=50 μm. All data are expressed as mean±standard deviation (SD). One-way analysis of variance, $^{**}P$<0.01 vs. WT group; $^{\#\#}P$<0.01 vs. 5×FAD group; $^{\&\&}P$<0.01 vs. Sham-tDCS group. White arrows indicate c-Fos positive cells. **c** Schematic representation and statistical results of cerebral blood volume (CBV) changes (ΔCBV) after tDCS intervention in the tDCS and Sham-tDCS group (n=3). Independent samples t-test, $^{\&}P$<0.05 vs. Sham-tDCS group. **d** Sequence of CBV changes after tDCS intervention (n=3). **e** Power spectral density from 0–30 Hz in left PFC after tDCS intervention (n=6). **f** Power spectral density from 30–48 Hz in left PFC after tDCS intervention (n=6). WT. Wild-type; 5×FAD. Transgenic mice with 5 familial AD

tDCS stimulation of the left PFC decreased Aβ deposition and regulated synaptic vesicle fusion and release probability in 5×FAD mice

Previous study has established Aβ plaque deposition as a pathognomonic feature of early AD [33]. To evaluate the effect of tDCS intervention on early AD pathology, we examined Aβ plaque deposition and Aβ42 protein expression levels in the left PFC of 5×FAD mice post-tDCS intervention. The results of both thioflavin staining and Western blotting experiments revealed that no Aβ plaques and Aβ42 protein expression were found in the left PFC of the WT group mice. In contrast, significant Aβ-positive plaques and Aβ42 protein expression levels occurred in 5×FAD group mice. The tDCS group exhibited significantly fewer Aβ-positive plaques and Aβ42 protein expression levels than both the 5×FAD and Sham-tDCS groups. No significant difference emerged between Sham-tDCS and 5×FAD groups (Fig. 3a-b), indicating tDCS mitigates Aβ plaque deposition and Aβ42 protein expression levels in 5×FAD mice.

To investigate the impact of tDCS intervention on neurochemical changes within the left PFC of 5×FAD mice, we utilized ^{1}H-MRS to assess alterations in relevant neurochemicals in the left PFC following tDCS intervention (Fig. 3c). Crucially, tDCS treatment significantly elevated Glu and NAA levels while reducing Cho concentrations compared to both the 5×FAD and Sham-tDCS groups. No significant differences emerged between the 5×FAD and Sham-tDCS groups, indicating tDCS modulates excitatory neurotransmitter metabolism (Fig. 3c). Glu, the principal excitatory neurotransmitter in the central nervous system and found within excitatory neurons, is intrinsically associated with working memory [21]. Therefore, our research concentrated on these excitatory neurons.

Notably, the quantity of synaptic vesicles and their release probability directly reflect presynaptic membrane transport capacity, which is a critical determinant of synaptic transmission [13]. To further examine tDCS effects on synaptic vesicle fusion and release in the left PFC, we observed presynaptic vesicle distribution using TEM. The results showed that the WT group mice exhibited dense, abundant presynaptic vesicles. Conversely, 5×FAD, tDCS, and Sham-tDCS groups showed reduced vesicle numbers and sparser distributions. Although less dense than WT, the tDCS group showed higher presynaptic vesicle counts than both the 5×FAD and Sham-tDCS groups (Fig. 3d). These findings indicated that the number of left PFC presynaptic vesicles was reduced in 5×FAD mice, while tDCS intervention partially promoted their formation. Subsequently, we utilized electrophysiological assays to assess the probabilities of synaptic vesicle fusion and release. Input/output (I/O) curves can directly reflect the basic transmission efficacy of neuronal synapses, and the larger the value of I/O indicates the stronger the synaptic transmission [34]. Paired-pulse ratio (PPR) indirectly reflects the change in the probability of the release of excitatory neurotransmitters from presynaptic vesicles, and the lower the PPR represents the larger the probability of fusion and release [35]. Analysis of I/O curves revealed significant differences in synaptic transmission between groups. Mice in the 5×FAD group exhibited a pronounced reduction in I/O curve amplitude compared to the WT group across a range of stimulation currents from 10 μA to 70 μA. Notably, tDCS group mice showed significantly enhanced I/O curve amplitudes relative to both 5×FAD and Sham-tDCS groups, particularly above 40 μA stimulation. Under stimulation conditions of 40 μA, 50 μA, 60 μA, and 70 μA, the output voltage of the tDCS group was markedly higher than that of the 5×FAD and Sham-tDCS groups. Whereas, no significant differences in I/O curves were observed between 5×FAD and Sham-tDCS groups at any tested current magnitude (Fig. 3e). The PPR results showed that the PPR values of the mice in the 5×FAD group were significantly higher than those of the WT group under stimulation at all time intervals tested. tDCS significantly reduced PPR in 5×FAD mice at shorter intervals (10 ms, 20 ms, and 50 ms), yielding lower values than both 5×FAD and Sham-tDCS groups. The 5×FAD and Sham-tDCS groups showed no significant PPR differences at any interval (Fig. 3f). Collectively, these results demonstrate that tDCS enhances the probabilities of synaptic vesicle fusion and release in 5×FAD mice.

tDCS stimulation of the left PFC brain region increased neuronal excitability and calcium ion concentration in 5×FAD mice

Vesicle release is significantly modulated by presynaptic neuronal excitability. We recorded the response frequency of left PFC neurons in mice to depolarizing current-step stimulation using Patch-Clamp recordings to assess neuronal excitability. Current intensity increased from 0 to 120 pA in 10 pA increments, with action potential frequency quantified within 600-ms windows (Fig. 4a-c). The results showed that, compared with the WT group, 5×FAD group mice showed a significant decrease in the number of spikes under depolarizing current stimulation, indicating that the excitability of neurons in the left PFC of 5×FAD mice was weakened. In contrast, tDCS stimulation could significantly increase the firing activity of neurons in this brain area and improve excitability. Further

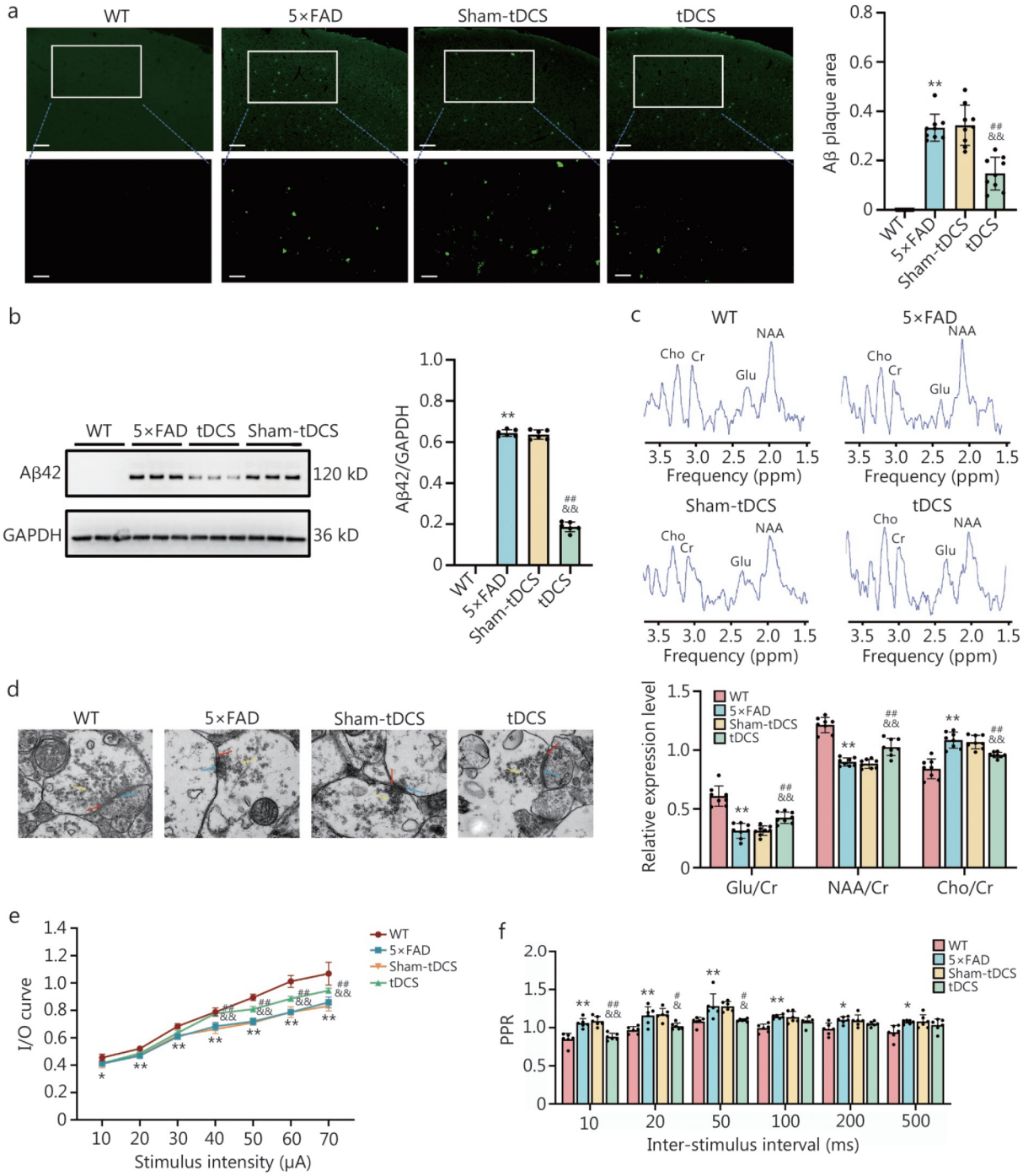

Fig. 3 Transcranial direct current stimulation (tDCS) stimulation of left prefrontal cortex (PFC) decreased amyloid β-protein (Aβ) deposition and regulated synaptic vesicle fusion and release probability in 5×FAD mice.

a Immunofluorescence pictures and statistical results of Aβ plaque deposition area in left PFC after tDCS intervention (n=9). Scale bar=200 μm (upper) and 100 μm (lower). **b** Western blotting analysis of Aβ42 expression levels in left PFC after tDCS intervention (n=6). **c** Relative expression level of glutamate (Glu), N-acetylaspartate (NAA), and choline (Cho) in left PFC after tDCS intervention (n=8). **d** Transmission electron microscopy (TEM) images of presynaptic vesicles in left PFC after tDCS intervention. The yellow arrows represent the presynaptic vesicle, the red arrows represent the synaptic cleft, and the blue arrows represent the postsynaptic density area. **e** Field potential recordings of input/output (I/O) curves in left PFC using Patch-Clamp (n=6). **f** Field potential recordings of paired-pulse ratio (PPR) in left PFC using Patch-Clamp (n=6). All data are expressed as mean±SD. Independent samples t-test and one-way analysis of variance, $^{*}P$<0.05, $^{**}P$<0.01 vs. WT group; $^{\#}P$<0.05, $^{\#\#}P$<0.01 vs. 5×FAD group; $^{\&}P$<0.05, $^{\&\&}P$<0.01 vs. Sham-tDCS group. WT. Wild-type; 5×FAD. Transgenic mice with 5 familial AD; Cr. Creatinine

analysis revealed that there was no statistically significant difference in the half-width and amplitude of action potentials between the groups (Fig. 4d). This suggests that tDCS may enhance action potential triggering efficiency by lowering neuronal excitation thresholds and is independent of changes in voltage-gated Na^+/K^+ channel function.

Through single-cell sequencing technology, we found that neurons accounted for the highest proportion of activated cell clusters in left PFC (Fig. 4e). Next, to investigate changes in excitatory neurons, we reannotated using the Glu marker genes solute carrier family 17 member 7 (SLC17A7) and SLC17A6, and found that glutamatergic neurons accounted for the majority of total neurons (Fig. 4f). Using Kyoto Encyclopedia of Genes and Genomes (KEGG) pathway and Gene Ontology (GO) pathway enrichment analysis, we found that KEGG enrichment was enriched in the p53 signaling pathway, axon guidance, and osteoclast differentiation pathways, pathways in cancer, mitogen-activated protein kinase (MAPK) signaling pathway, and Hippo signaling pathway, among others (Fig. 4g). GO_C enrichment included synapse, dendrite, neuronal cell body, axon, and glutamatergic synapse, while GO_F enrichment included transcription regulatory region sequence, protein binding, collagen binding, and ionotropic Glu receptor binding (Additional file 1: Fig. S1). Furthermore, we analyzed synapse vesicle-related genes in glutamatergic neurons and found that synaptosomal-associated 25 kD protein (Snap25), synaptotagmin-1 (Syt1), syntaxin 1A (STX1A), mammalian unc-13 homolog A (Munc13-1), and syntaxin-binding protein 1 (Munc18-1) were highly expressed in glutamatergic neurons, while vesicle associated membrane protein 2 (VAMP2) was only present in some clusters (Fig. 4h). These data indicate that tDCS may activate glutamatergic neurons. In addition, calcium fiber photometry experiments revealed that calcium ΔF/F and Z-scores were significantly lower in the 5×FAD group than in the WT group. Notably, calcium ΔF/F and Z-scores were significantly higher in the tDCS group than in the 5×FAD and Sham-tDCS groups. No statistically significant difference emerged between the Sham-tDCS and 5×FAD groups (Fig. 4i). These data indicate that tDCS increases calcium ion concentration in the left PFC of 5×FAD mice, enhancing neuronal discharge activity and excitability, and that is associated with excitatory neurons.

Opt treatment on the left PFC improved working memory and synaptic vesicle fusion and release probability in 5×FAD mice

In the central nervous system, the vast majority of excitatory neurons are glutamatergic neurons. Given our finding that tDCS activated excitatory (predominantly glutamatergic) neurons, the results suggested that glutamatergic neuronal population might be a primary cellular target for tDCS. We therefore employed an optogenetic strategy to test if activating this population was sufficient to rescue working memory deficits, thereby investigating the connection between tDCS-mediated improvement in AD-related working memory and synaptic transmission in excitatory neurons of the left PFC. Specifically, we injected the left PFC with an adeno-associated virus [rAAV-CaMKIIa-hChR2(H134R)-mCherry-WPRE-hGH polyA]. This allowed precise activation of glutamatergic neurons in the left PFC using 473 nm blue light (Fig. 5a). Before Opt intervention, the T-maze results showed that the autonomous alternation rate of 5×FAD mice was significantly lower than that of the WT group. The baseline level was consistent across the 5×FAD, Sham-Opt, and Opt groups (Fig. 5b). This deficit indicates impaired working memory and demonstrates an early manifestation of AD-related cognitive decline. After Opt stimulation of the left PFC, the autonomous alternation rate of the T-maze in 5×FAD mice was improved (Fig. 5b). We also used the MWM test to detect the effect of Opt stimulation of the left PFC on working memory in mice. MWM testing likewise demonstrated significant working memory enhancement in the Opt group mice, corroborating T-maze findings (Fig. 5c). These results indicate that Opt stimulation targeting left PFC glutamatergic neurons improves cognitive function.

To assess the impact of Opt stimulation on neurochemical changes within the left PFC, we employed ^{1}H-MRS to monitor alterations in relevant neurochemicals in left PFC (Fig. 5d). Compared with the WT group, 5×FAD group mice had lower levels of Glu and NAA and higher levels of Cho (Fig. 5d). After Opt stimulation, Glu and NAA levels were up-regulated and Cho levels were down-regulated in the Opt group compared with the 5×FAD and Sham-Opt groups. There was no significant difference between the 5×FAD and Sham-Opt groups, suggesting that Opt stimulation affects left PFC excitatory neurotransmitter metabolism.

To investigate whether the activation of glutamatergic neurons in left PFC influences synaptic vesicle fusion and release, we utilized TEM to examine the number of synaptic vesicles in the presynaptic membrane and electrophysiological recordings to assess the probability of vesicle release. The results showed that the presynaptic vesicles in the left PFC of the 5×FAD group were sparsely arranged. The number of vesicles was significantly reduced compared with WT group (Fig. 5e). After 7 d of Opt stimulation, the number of left PFC presynaptic vesicles in the Opt group was significantly

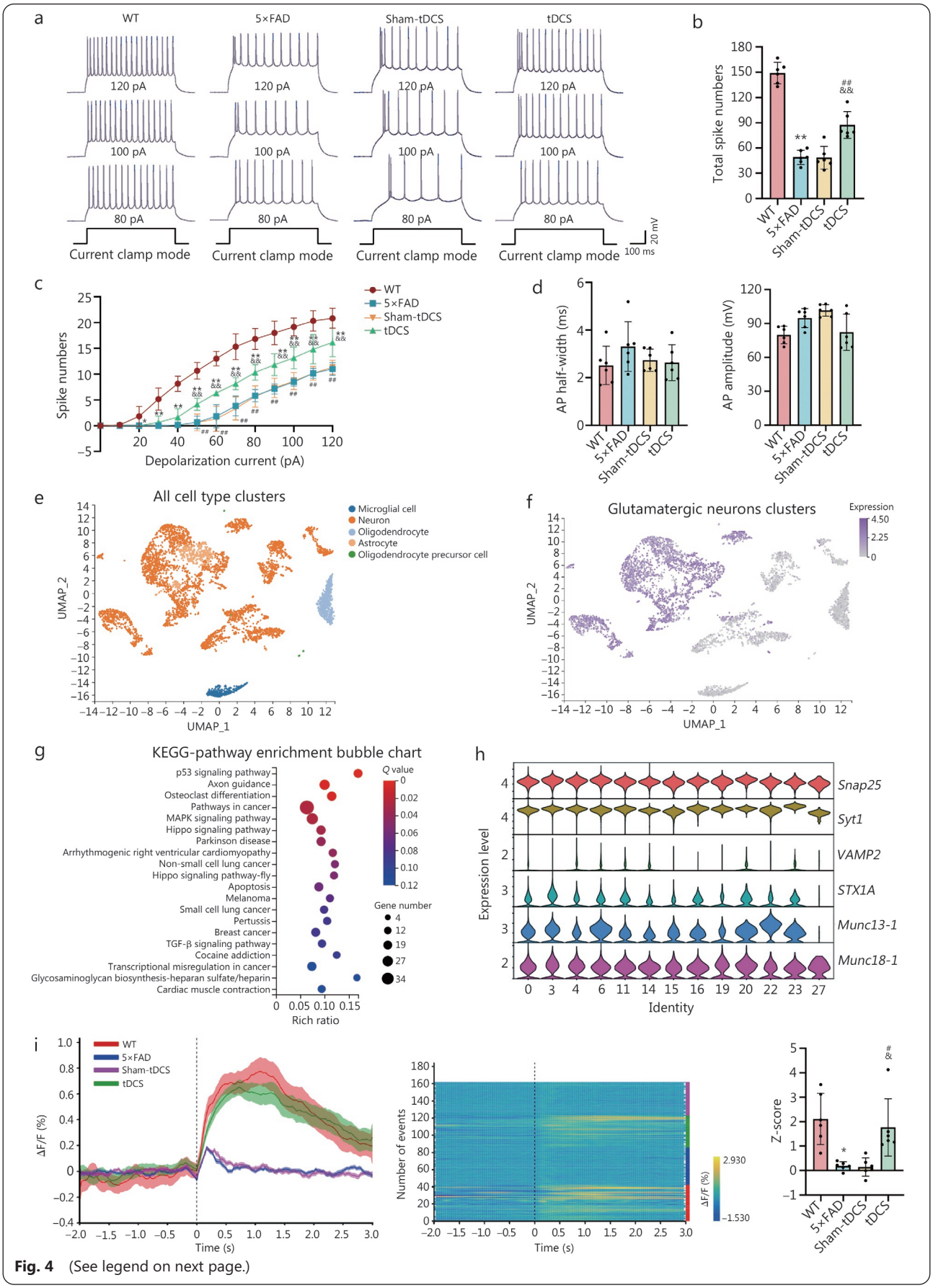

Fig. 4 (See legend on next page.)

(See figure on previous page.)

Fig. 4 Transcranial direct current stimulation (tDCS) stimulation of the left prefrontal cortex (PFC) increased neuronal excitability and calcium ion concentration in 5×FAD mice.

a Representative traces from the excitatory neurons in response to current injections in left PFC after tDCS intervention. **b** Comparison of the total number of spikes at 0–120 pA depolarization current in left PFC after tDCS intervention (n=6). **c** The relationship curve between depolarization current of different intensities and the number of spikes (n=6). **d** Comparison of peak average half wave width (n=6) and amplitude (n=6) at 0–120 pA depolarization current in left PFC after tDCS intervention. **e** Uniform manifold approximation and projection (UMAP) visualization of cell clustering results from left PFC after tDCS intervention. **f** Left PFC cell marker gene annotation results UMAP display diagram after tDCS intervention. **g** Kyoto Encyclopedia of Genes and Genomes (KEGG) pathway enrichment bubble chart after tDCS intervention. **h** Gene expression in glutamate synapses after tDCS intervention. **i** Fluorescence change values (ΔF/F) of calcium fiber and Z-score of calcium fiber in left PFC after tDCS intervention (n=6). Except for Z-scores, which are expressed as the median (interquartile range), all data are expressed as mean±SD. One-way analysis of variance and Kruskal-Wallis test, $^{*}P<0.05$, $^{**}P<0.01$ vs. WT group; $^{\#}P<0.05$, $^{\#\#}P<0.01$ vs. 5×FAD group; $^{\&}P<0.05$, $^{\&\&}P<0.01$ vs. Sham-tDCS group. WT. Wild-type; 5×FAD. Transgenic mice with 5 familial AD; Snap25. Synaptosomal-associated 25 kD protein; Syt1. Synaptotagmin-1; STX1A. Syntaxin 1A; VAMP2. Vesicle associated membrane protein 2; Munc13-1. Mammalian unc-13 homolog A; Munc18-1. Syntaxin-binding protein 1; AP. Action potentials; MAPK. Mitogen-activated protein kinase; TGF. Transforming growth factor

increased, arranged centrally, and distributed tightly compared with the 5×FAD and Sham-Opt groups (Fig. 5e). The images of the 5×FAD and Sham-Opt groups showed a similar pattern of distribution and number of vesicles. Subsequently, we assessed the effects of Opt activation of glutamatergic neurons on synaptic efficacy and vesicular release in the left PFC by recording I/O curves and PPR in each group. Analysis of I/O curves revealed that the Opt group exhibited significantly elevated output voltage (fEPSP amplitude) compared to both the 5×FAD and Sham-Opt groups, with statistically significant differences emerging at stimulation intensities beyond 40 μA (Fig. 5f). The PPR was significantly lower in the Opt group compared to the 5×FAD and Sham-Opt groups at shorter intervals (20 ms, 50 ms, and 100 ms) (Fig. 5g). Similarly, we found no statistically significant difference in PPR between the 5×FAD and Sham-Opt groups. To investigate the role of excitatory neurons activated by tDCS, we used optogenetics to selectively stimulate this population in the left PFC. This targeted activation enhanced synaptic transmission and rescued early AD-related working memory deficits, demonstrating that cognitive improvement is coupled to potentiated synaptic efficacy. Overall, our results provide further support for the conclusion that the therapeutic effect of tDCS is achieved through the activation of this excitatory neuronal population.

tDCS stimulation of the left PFC brain regions upregulated synaptic vesicle transport-associated proteins in 5×FAD mice

Aware that tDCS can enhance the fusion and release of synaptic vesicles, and given the pivotal role of the SNARE complex in vesicular transport, we employed non-denaturing Western blotting analysis to investigate the impact of tDCS intervention on the assembly levels of the SNARE complex. The results showed that SNARE complex formation was significantly reduced in the 5×FAD group compared with the WT group. The level of SNARE complex formation was significantly elevated in the tDCS group compared with the 5×FAD and Sham-tDCS groups. There was no difference in the 5×FAD group compared with the Sham-tDCS group (Fig. 6a). Subsequently, in our quest to elucidate the effects of tDCS intervention on the SNARE complex and its chaperone molecules in 5×FAD mice, we examined the expression levels of Snap25 and Syt1. The expression levels of Snap25 and Syt1 proteins were elevated in the tDCS group compared to the 5×FAD and Sham-tDCS groups (Fig. 6b). The same was observed in the Opt group (Fig. 6c). These data indicated that tDCS stimulation up-regulated the expression levels of SNARE complex and chaperone molecule-related proteins in 5×FAD mice.

SNARE interference virus decreased working memory and synaptic vesicle fusion and release in 5×FAD mice

To delineate the role of the SNARE complex and its chaperone molecules in the ameliorative effects of tDCS on early AD-related working memory deficits and synaptic vesicle fusion and release, we utilized recombinant adeno-associated virus (rAAV)-mediated SNARE interference viruses. rAAV-mediated SNARE-inhibitory viruses or control viruses were used for the left PFC in the experiments (Fig. 6d). First, we checked the accuracy of the rAAV injection location, and EGFP expression in the left PFC region could be clearly seen under fluorescence microscopy (Fig. 6d). Second, the working memory of each group before and after tDCS intervention was examined by the spontaneous alternating experimental behavior of the Y-maze test. The results of the pre-intervention Y-maze test showed that there was no difference in the spontaneous alternation rate of 5×FAD mice between the groups, indicating that the level

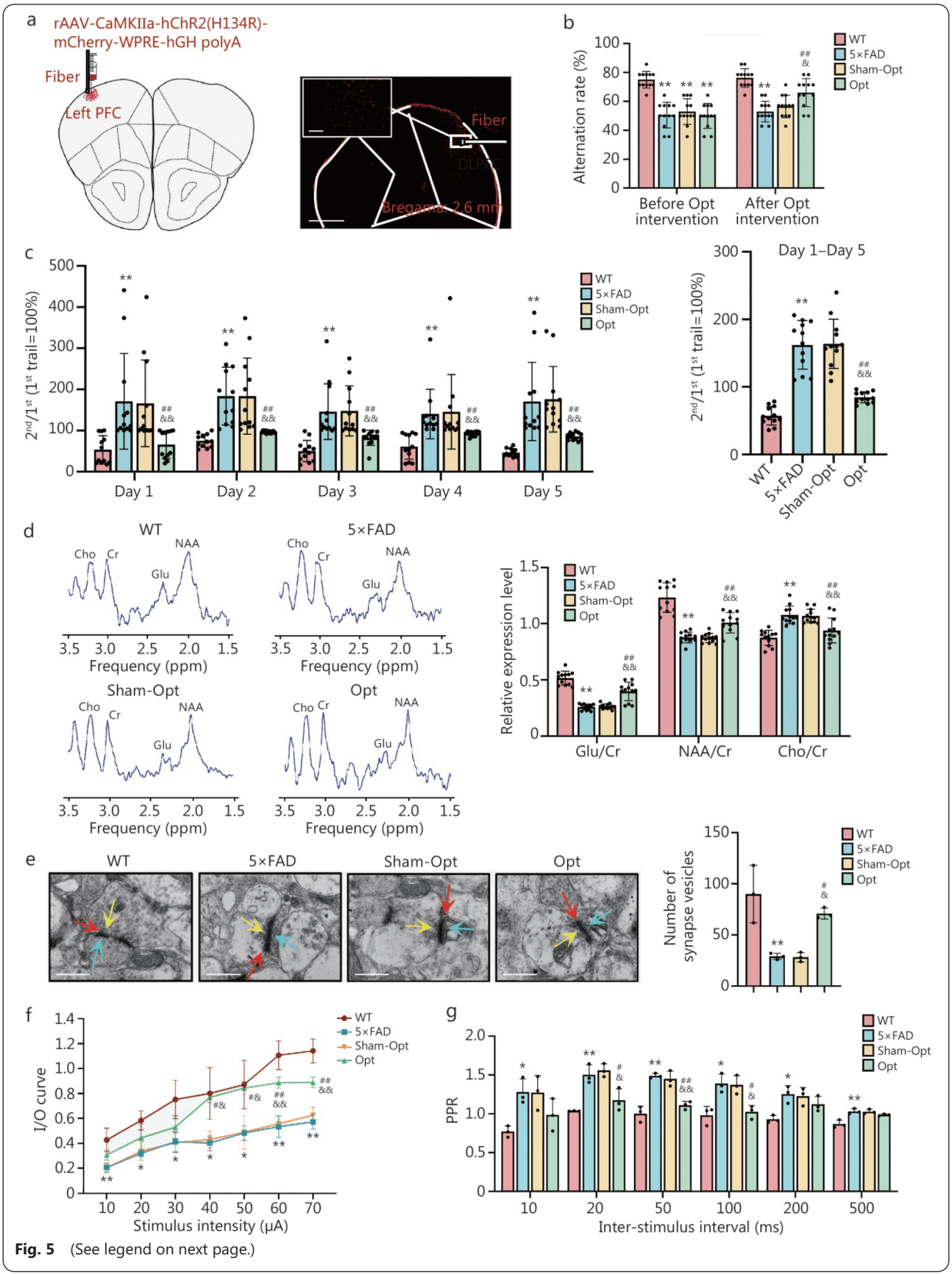

Fig. 5 (See legend on next page.)

(See figure on previous page.)

Fig. 5 Optogenetic (Opt) stimulation of left prefrontal cortex (PFC) improved working memory function and synaptic vesicle fusion and release probability in 5×FAD mice.

a Schematic diagram of Opt viruses injection and expression in left PFC. The red position indicated successful expression of the Opt viruses. Scale bar=500 μm in panoramic views and 100 μm in enlarged images. **b** Spontaneous alternation rate of T-maze before Opt intervention (n=12) and after Opt intervention (n=12). **c** The ratio of the second day to the first day of the working memory morris water maze (MWM) avoidance latency period after Opt intervention (n=12). **d** Relative expression level of glutamate (Glu), N-acetylaspartate (NAA), and choline (Cho) in left PFC after Opt intervention (n=12). **e** Transmission electron microscopy (TEM) images of presynaptic vesicles and quantification of presynaptic vesicles number in left PFC (n=3). The yellow arrows represent the presynaptic vesicle, the red arrows represent the synaptic cleft, and the blue arrows represent the postsynaptic density area. Scale bar=500 nm. **f** Field potential recordings of input/output (I/O) curves in left PFC using Patch-Clamp (n=3). **g** Field potential recordings of paired-pulse ratio (PPR) in left PFC using Patch-Clamp (n=3). All data are expressed as mean±SD. One-way analysis of variance, $^{*}P<0.05$, $^{**}P<0.01$ vs. WT group; $^{\#}P<0.05$, $^{\#\#}P<0.01$ vs. 5×FAD group; $^{\&}P<0.05$, $^{\&\&}P<0.01$ vs. Sham-Opt group. WT. Wild-type; Cr. Creatinine

of working memory was consistent in all groups before tDCS intervention (Fig. 6e). After intervention, Y-maze spontaneous alternation rate in the tDCS+tettoxlc group was lower than the tDCS and tDCS+EGFP groups, whereas no intergroup differences were seen between the tDCS and tDCS+EGFP groups (Fig. 6e). In the MWM test, compared with the tDCS and tDCS+EGFP groups, the ratio of the second to the first escape latency from day 1 to day 5 swas significantly increased in the tDCS+tettoxlc group, with the difference being statistically significant (Additional file 1: Fig. S2a). The average ratio of the second to first escape latency over the 5 d was also significantly increased in the tDCS+tettoxlc group (Additional file 1: Fig. S2a). Additionally, the results of the NOR test revealed that the discrimination index was significantly reduced in the tDCS+tettoxlc group (Additional file 1: Fig. S2b). The above results indicated that SNARE-inhibitory viruses weakened the improvement effect of tDCS on AD working memory, suggesting that SNARE complexes are involved in the alleviation of early AD-related working memory deficits by tDCS-stimulated left PFC in 5×FAD mice.

Further, we used non-denaturing Western blotting to detect the efficiency of SANRE complex silencing. The results showed that the level of SANRE complex formation in the tDCS+tettoxlc group was significantly lower than the tDCS and tDCS+EGFP groups, whereas there was no difference between the tDCS and tDCS+EGFP groups (Fig. 6f). This showed the successful inhibitory effect of the SNARE interference virus on the level of SNARE complex formation.

To assess the impact of SNARE-interference virus on tDCS-mediated synaptic vesicle fusion and release probabilities, we used electrophysiological techniques to record I/O values in the left PFC of mice. Subsequently, we plotted I/O curves and PPR values to evaluate the alterations in synaptic vesicle fusion and release. Our results indicate that the output voltages of the tDCS+tettoxlc group were significantly lower than those of the tDCS and tDCS+EGFP groups. Furthermore, the voltage values of the tDCS+tettoxlc group decreased significantly starting from 30 μA. In contrast, no significant differences in I/O values were observed between the tDCS and tDCS+EGFP groups across all tested stimulation intensities (Fig. 6g). PPR results showed that at time intervals of 50 ms, 100 ms, and 200 ms for stimulation, the PPR of mice in the tDCS+tettoxlc group was significantly higher than the tDCS and tDCS+EGFP groups, while the difference in PPR between the tDCS and tDCS+EGFP groups under stimulation at any time interval was not significant (Fig. 6h). In addition, calcium ΔF/F and Z-scores experiments revealed a significant decrease in the tDCS+tettoxlc group compared to the tDCS and tDCS+EGFP groups (Fig. 6i). These data demonstrated that SNARE interference virus reduced the enhancement of synaptic vesicle fusion and release conferred by tDCS in 5×FAD mice. This suggested that SNARE complexes mediated the process through which tDCS stimulation of the left PFC enhanced synaptic vesicle fusion and release.

Snap25 is on the presynaptic membrane, and VAMP2 is located on the synaptic vesicle membrane. The docking and subsequent fusion of synaptic vesicles with the presynaptic membrane, facilitated by the interaction between these two proteins, trigger neurotransmitter release [36,37]. To determine whether SNARE complex inhibition alters tDCS-mediated regulation of presynaptic vesicle fusion, we evaluated Snap25 and VAMP2 colocalization using immunofluorescence. Analysis revealed overlapping fluorescence signals, evidenced by yellow emission where Snap25 (red) and VAMP2 (green) co-localized. Specifically, the tDCS+tettoxlc group exhibited attenuated VAMP2 green fluorescence and reduced, fainter yellow co-localization areas compared to tDCS and tDCS+EGFP groups. Pearson's correlation analysis indicated weak colocalization between Snap25 and VAMP2 in the tDCS+tettoxlc group (r<0.5),

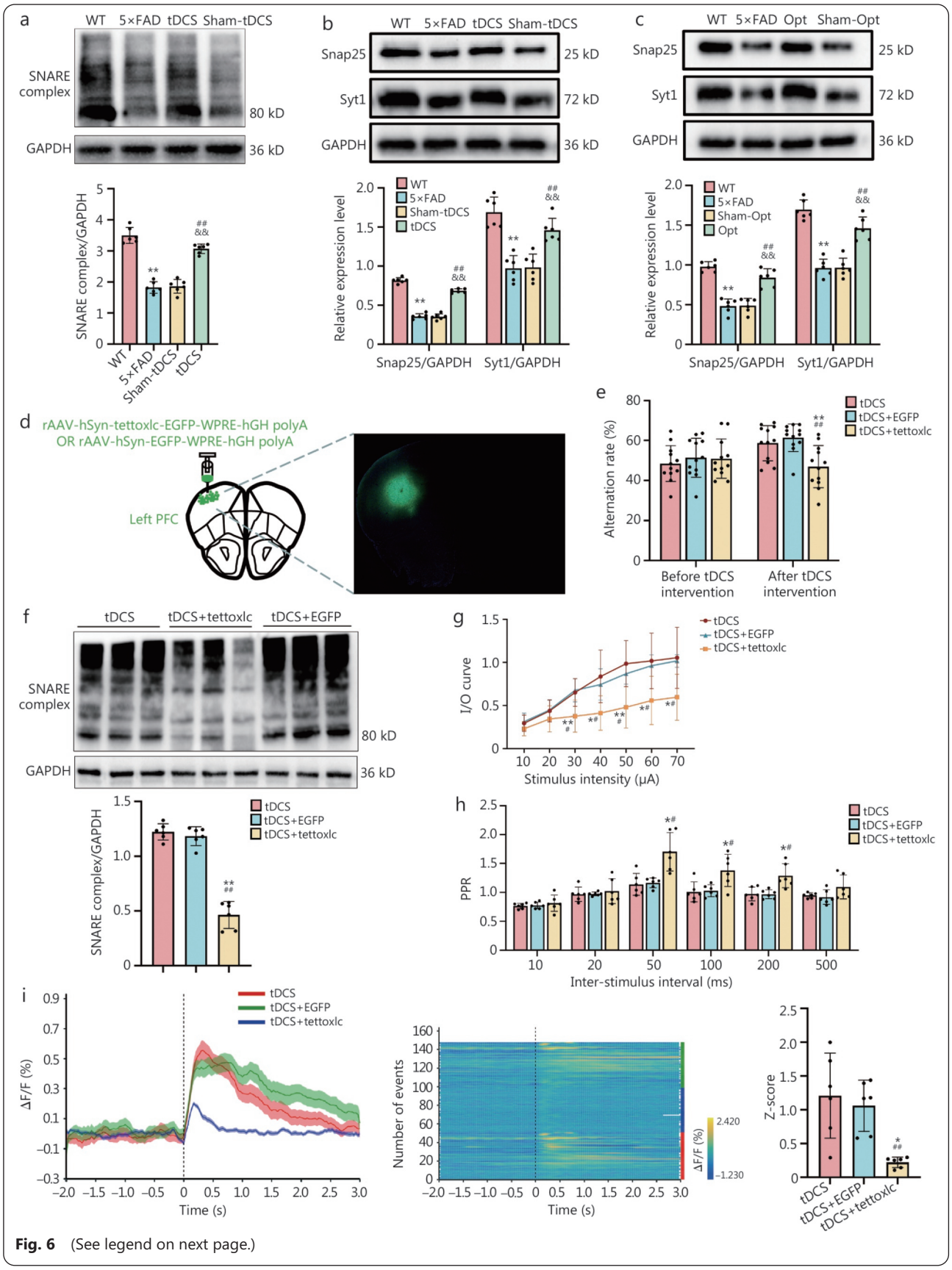

Fig. 6 (See legend on next page.)

(See figure on previous page.)

Fig. 6 Transcranial direct current stimulation (tDCS) stimulation of left prefrontal cortex (PFC) upregulated synaptic vesicle transport-associated proteins in 5×FAD mice.

a Western blotting analysis of soluble N-ethylmaleimide-sensitive factor attachment receptor (SNARE) complex expression levels in left PFC after tDCS intervention (n=6). One-way analysis of variance, $^{**}P$<0.01 vs. WT group; $^{\#\#}P$<0.01 vs. 5×FAD group; $^{\&\&}P$<0.01 vs. Sham-tDCS group. **b** Western blotting analysis of synaptosomal-associated 25 kD protein (Snap25) and synaptotagmin-1 (Syt1) expression levels in left PFC after tDCS intervention (n=6). One-way analysis of variance, $^{**}P$<0.01 vs. WT group; $^{\#\#}P$<0.01 vs. 5×FAD group; $^{\&\&}P$<0.01 vs. Sham-tDCS group. **c** Western blotting analysis of Snap25 and Syt1 expression levels in left PFC after Optogenetic (Opt) intervention (n=6). One-way analysis of variance, $^{**}P$<0.01 *vs*. WT group; $^{\#\#}P$<0.01 vs. 5×FAD group; $^{\&\&}P$<0.01 vs. Sham-Opt group. **d** Schematic diagram of SNARE-inhibitory viruses injection and expression in left PFC. The green position indicated successful expression of the SNARE-inhibitory viruses. **e** Spontaneous alternation rate of Y-maze before tDCS intervention (n=12) and after tDCS intervention (n=12). One-way analysis of variance, $^{**}P$<0.01 vs. tDCS group; $^{\#\#}P$<0.01 vs. tDCS+EGFP group. **f** Western blotting analysis of SNARE complex expression levels in left PFC (n=6). One-way analysis of variance, $^{**}P$<0.01 vs. tDCS group; $^{\#\#}P$<0.01 vs. tDCS+EGFP group. **g** Field potential recordings of input/output (I/O) curves in left PFC using Patch-Clamp (n=6). One-way analysis of variance, $^{*}P$<0.05, $^{**}P$<0.01 vs. tDCS group; $^{\#}P$<0.05 vs. tDCS+EGFP group. **h** Field potential recordings of paired-pulse ratio (PPR) in left PFC using Patch-Clamp (n=6). One-way analysis of variance, $^{*}P$<0.05 vs. tDCS group; $^{\#}P$<0.05 vs. tDCS+EGFP group. **i** Fluorescence change values (ΔF/F) of calcium fiber and Z-score of calcium fiber in left PFC (n=6). One-way analysis of variance, $^{*}P$<0.05 vs. tDCS group; $^{\#\#}P$<0.01 vs. tDCS+EGFP group. All data are expressed as mean±standard deviation (SD). WT. Wild-type; 5×FAD. Transgenic mice with 5 familial AD; EGFP. Enhanced green fluorescent protein

whereas significant colocalization was observed in the tDCS (r=0.546) and tDCS+EGFP (r=0.604) groups (Fig. 7a). The results indicated that tDCS applied to the left PFC enhanced synaptic vesicle fusion in 5×FAD mice, which was abolished by the administration of an SNARE interference virus. This finding confirmed that SNARE complexes mediated the process through which tDCS stimulation of left PFC promoted synaptic vesicle fusion levels.

To investigate the impact of SNARE complex inhibition on the modulatory effects of tDCS on the SNARE complex and its chaperone molecules, we utilized Western blotting analysis to assess the expression levels of monomeric proteins within the SNARE complex, including STX1A, Snap25, and VAMP2, as well as chaperone proteins Munc13-1, Munc18-1, and Syt1 in the left PFC of mice following tDCS intervention. The Western blotting results showed that, compared with the tDCS and tDCS+EGFP groups, the expression levels of VAMP2, Munc13-1, and Syt1 were decreased, and STX1A were increased in the tDCS+tettoxlc group, whereas there was no difference in Snap25 and Munc18-1. There was no significant difference in the expression of each protein in the tDCS group compared with the tDCS+EGFP group (Fig. 7b-c). Next, we employed Co-IP to investigate the interactions between the SNARE complex and its chaperone molecules. Snap25 and Syt1 interactions are involved in the SNARE-mediated synaptic membrane fusion process [38], whereas the binding of STX1A to Munc18-1 inhibits the formation of the SNARE complex [39]. The Co-IP results showed that in the tDCS+tettoxlc group, the protein interactions between Snap25 and Syt1 were significantly reduced, while those between STX1A and Munc18-1 were significantly enhanced, as compared to both the tDCS and tDCS+EGFP groups. No statistically significant differences in protein interactions were observed between the tDCS and tDCS+EGFP groups (Fig. 7d-e). The above results indicated that tDCS stimulation modulated protein interactions between SNARE complexes and chaperone molecules in the left PFC of 5×FAD mice, thereby regulating synaptic vesicle fusion and release.

Discussion

Working memory impairment is particularly prominent in the early stages of AD and and severely affects patients' quality of life [40]. Clinical studies have shown that tDCS applied to the left PFC can improve working memory performance in AD patients [9], however, the specific neurobiological mechanisms remain unclear. Our study found that tDCS stimulation of the left PFC activates excitatory neurons, promoted presynaptic vesicle fusion and glutamate release, and thereby ameliorates working memory deficits in early-stage AD model mice. Opt stimulation provided more accurate confirmation that activating left PFC excitatory neurons and the resulting presynaptic vesicle fusion and glutamate release were crucial for ameliorating early AD-related working memory deficits. We identified the SNARE complex and its chaperone molecules as key regulators that promote synaptic vesicle fusion and glutamate release and we indicated that tDCS enhanced the interactions between the SNARE complex and its chaperone molecules, thereby promoting synaptic vesicle fusion and glutamate release. Our work provides mechanistic insights and scientific evidence to support the clinical application of tDCS (Fig. 8).

AD is a progressive neurodegenerative disorder charac-

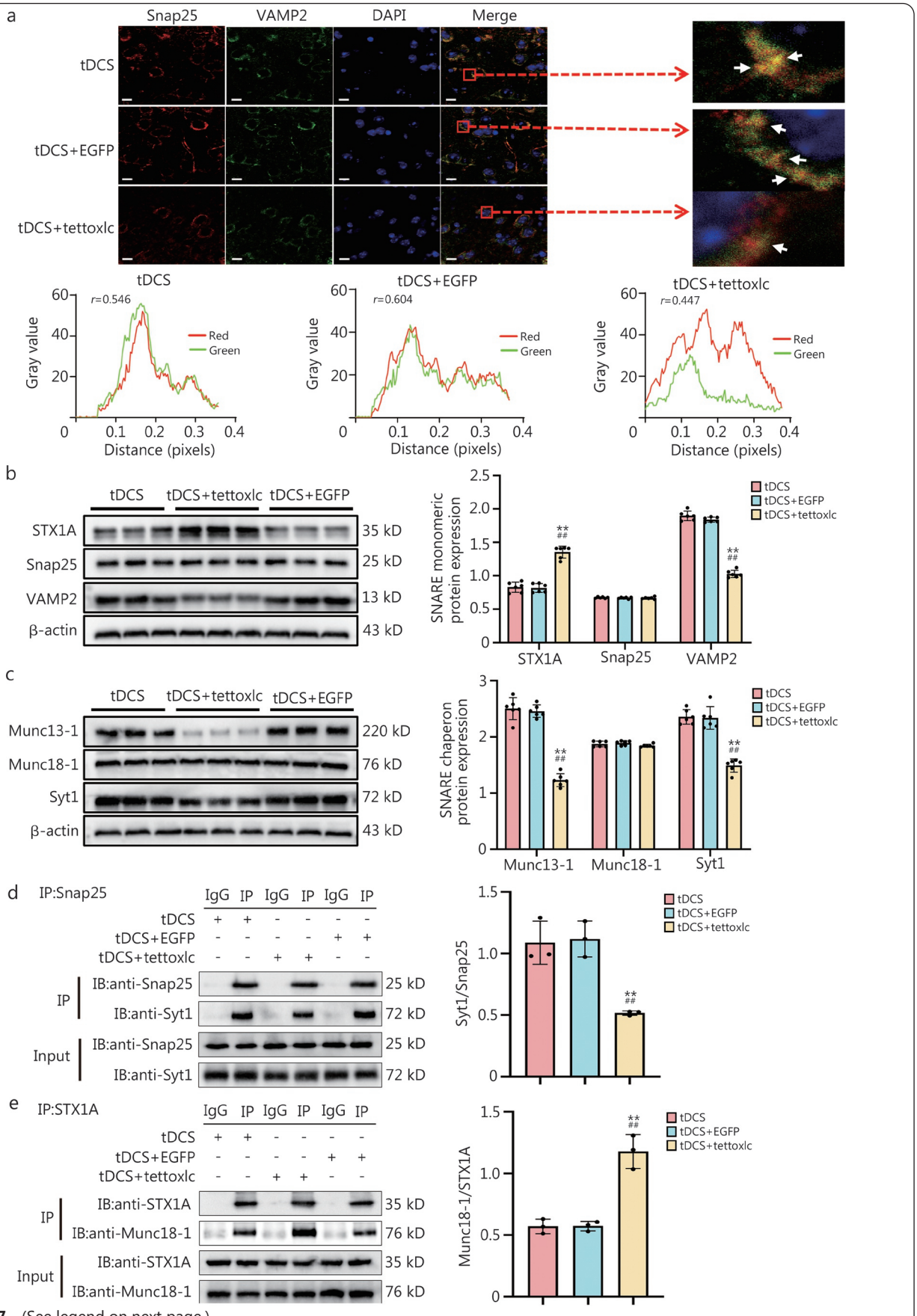

Fig. 7 (See legend on next page.)

(See figure on previous page.)

Fig. 7 Soluble N-ethylmaleimide-sensitive factor attachment receptor (SNARE)-inhibitory viruses decreased working memory function and synaptic vesicle fusion and release in 5×FAD mice.

a Co-localization of synaptosomal-associated 25 kD protein (Snap25) and vesicle associated membrane protein 2 (VAMP2) in left prefrontal cortex (PFC) and local enlarged view. The yellow position indicated by the arrows is the co-locating part. Scale bar=10 μm. Pearson's correlation analysis indicated weak colocalization between Snap25 and VAMP2 in the tDCS+tettoxlc group (r<0.5). **b** Western blotting analysis of syntaxin 1A (STX1A), Snap25, and VAMP2 expression levels in left PFC (n=6). **c** Western blotting analysis of mammalian unc-13 homolog A (Munc13-1), syntaxin-binding protein 1 (Munc18-1), and synaptotagmin-1 (Syt1) expression levels in left PFC (n=6). **d** Co-immunoprecipitation (Co-IP) analysis of the interaction of between Sty1 and Snap25 in left PFC (n=3). **e** CO-IP analysis of the interaction of between Munc18-1 and STX1A in left PFC (n=3). All data are expressed as mean±SD. One-way analysis of variance, $^{**}P$<0.01 vs. tDCS group; $^{\#\#}P$<0.01 vs. tDCS+EGFP group. tDCS. Transcranial direct current stimulation; Co-IP. Co-immunoprecipitation; EGFP. Enhanced green fluorescent protein

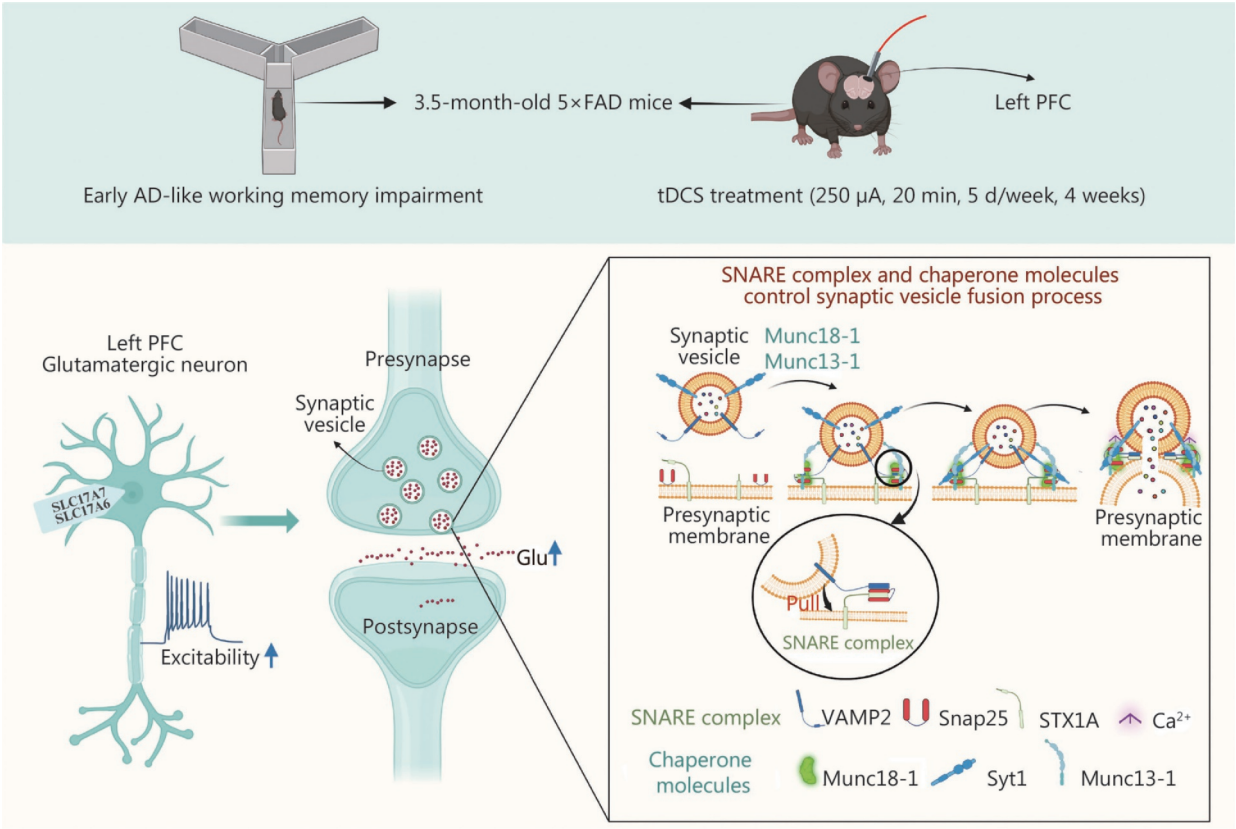

Fig. 8 Schematic model illustrating the mechanism of transcranial direct current stimulation (tDCS) in improving working memory in early Alzheimer's disease (AD)-like mice.

tDCS applied over the left prefrontal cortex (PFC) activated excitatory neurons, which promoted the interaction between the soluble N-ethylmaleimide-sensitive factor attachment receptor (SNARE) complex and its chaperone molecules. This enhanced synaptic vesicle fusion and glutamate release, ultimately improving working memory in early AD-like mice. SLC17A7. Solute carrier family 17 member 7; SLC17A6. Solute carrier family 17 member 6; Glu. Glutamate; Munc13-1. Mammalian unc-13 homolog A; Munc18-1. Syntaxin-binding protein 1; VAMP2. Vesicle associated membrane protein 2; Snap25. Synaptosomal-associated 25 kD protein; Syt1. Synaptotagmin-1; STX1A. Syntaxin 1A

terized by cognitive decline, with working memory impairment manifesting during early disease stages [41]. Clinical investigations demonstrated that people with early AD performed worse on working memory tasks compared to healthy older adults [42]. Similarly, this result was validated in animal studies, as evidenced by increased error rates in 3-month-old AD model mice compared to WT controls during 8-arm maze working memory assessments [43]. This is consistent with our results. The 5×FAD mice model, Mo/HuAPP695swe and PS1-dE9 (APP/PS1) transgenic mice harboring 5 familial AD gene mutations, recapitulates key pathological features of human AD. Our study confirmed that 3.5-month-old 5×FAD mice exhibited working memory deficits concurrent with elevated Aβ plaque deposition, closely

mirroring the clinicopathological profile of early human AD. Therefore, 5×FAD mice at this age served as a model of early AD pathogenesis and were selected for this study [44]. To avoid potential confounding effects from hormone fluctuations associated with the estrous cycle in female animals, this study exclusively utilized male mice, thereby limiting the generalizability of the findings to female mice. Left DLPFC activation enhances accuracy and reduces reaction time in working memory tasks [45]. Thus, the left DLPFC serves not only as a key brain region for working memory execution, but also as a therapeutic target for cognitive enhancement, motivating its selection as our intervention target.

In recent years, numerous studies have revealed that non-invasive brain stimulation, particularly tDCS targeting DLPFC, effectively ameliorates working memory impairment [9,46]. Present study utilized stereotaxic targeting of the murine PFC, a region exhibiting functional homology with the primate DLPFC in cognitive processes such as working memory, because there is no discrete DLPFC parcellation in murine neuroanatomy. Given the well-established crucial role of the rodent PFC in working memory processes [47], in the present study, we performed a 4-week anodic tDCS intervention on the left PFC of 3.5-month-old 5×FAD mice and found that the intervention ameliorated working memory deficits in early AD model mice while enhancing left PFC blood flow, neuronal excitability, and the activation of excitatory neurons. These observations suggested that excitatory neurons may be a key target through which tDCS improves working memory deficits in early AD. Synaptic transmission is essential for working memory processes [19]. Neuronal excitation is an important driver of Glu release [48] and that our results further showed tDCS increased synaptic transmission and Glu release, we proceeded to explore the relationship between excitatory neurons, synaptic transmission, and working memory improvement. Opt, a neuromodulation technique with high temporal and spatial resolution, has been widely used in studies examining the working mechanisms of neural circuits. This technique can precisely target specific brain regions with exceptional spatiotemporal precision and selectively excite or inhibit specific neuronal populations, producing therapeutic benefits [49]. Previous research demonstrated that Opt activation of prefrontal cortical neurons improved task performance and rescued synaptic dysfunction during delayed working memory tasks in rodents [50]. We found that tDCS predominantly activates glutamatergic neurons, the principal excitatory subtype in the central nervous system [48]. Therefore, building upon this foundation, we employed optogenetic strategies to selectively activate left PFC glutamatergic neurons in 5×FAD mice. We found that targeted activation of left PFC glutamatergic neurons promoted synaptic transmission and glutamate release, thereby ameliorating working memory deficits in early AD model mice. This further supports the conclusion that the improvement in working memory induced by tDCS is closely related to the activation of excitatory neurons and the synaptic transmission they mediate.

It should be noted that in our study, tDCS intervention did not significantly change the percentage of all frequency bands. The absence of significant EEG alterations in our study likely stems from two principal considerations. First, although our findings showed no statistically significant differences between the Sham-tDCS group and the non-surgical AD control group, it cannot be ruled out that the implant surgery itself, applied to both the sham surgery group and the tDCS group, may have induced brain changes. This could be one reason why tDCS did not significantly alter EEG frequency. Second, brain exhibits intricate interactions among neural circuits. Consequently, localized left PFC stimulation may not elicit detectable changes in electrical activity at the macroscopic level, thus accounting for the absence of significant alterations captured by EEG.

Furthermore, our study observed that tDCS was able to reduce Aβ deposition in AD model mice. Although our experimental results did not establish a clear relationship between reduced Aβ deposition and increased presynaptic vesicle release in excitatory neurons, we observed that tDCS stimulation activated astrocytes, which may contribute to decreased Aβ accumulation. The role of astrocytes in AD is highly nuanced. They act as "scavengers", clearing toxic proteins such as Aβ [51]. Notably, the recent discovery of the glymphatic system, an astrocyte-mediated waste clearance pathway in the brain, has underscored the central role of astrocytes in maintaining brain health [52]. The glymphatic system relies on aquaporin-4 (AQP4) water channels located on astrocytic endfeet to facilitate the convective exchange between cerebrospinal fluid and interstitial fluid, thereby promoting the clearance of metabolic wastes, including Aβ, from the brain parenchyma [53]. Therefore, in our study, tDCS may enhance Aβ clearance by activating astrocytes and potentially the glymphatic system. That said, the reduction of Aβ deposition involves multifaceted mechanisms, warranting further in-depth investigation. These results collectively point to the beneficial effects of tDCS in the early stages of AD.

Synaptic vesicle fusion and release constitute the critical initial step in signal transmission of excitatory neurons and serve as the neurophysiological basis for working memory encoding [54]. Impairment of this function disrupts high-

frequency neuronal firing and oscillatory network activity in the prefrontal cortex, thereby leading to working memory deficits [55]. Notably, both early-stage AD patients and AD model animals exhibit impairments in synaptic vesicle fusion and release [56-58]. In excitatory neurons, this process is precisely regulated by the SNARE complex (composed of VAMP2, STX1A, and SNAP25) and its chaperone proteins, such as Munc18-1, Munc13-1, and Syt1 [59,60]. Before SNARE complex formation, Munc18-1 binds specifically to the Habc and H3 domains of STX1A, inducing a closed conformation through opposite-directional folding. This structure allosterically inhibits SNARE complex assembly by restricting STX1A interactions with VAMP2 and Snap25 [39]. During synaptic vesicle exocytosis initiation, Munc13-1 mediates STX1A conformational opening via its MUN domain, catalyzing Munc18-1 and facilitating the dissociation of Munc18-1 from STX1A, placing STX1A in an activated state and promoting SNARE complex formation [61,62]. STX1A and VAMP2 each contribute one α-helix, while VAMP2 provides two additional α-helices, forming a "zipper-like" rod-shaped four-helix bundle [63]. The force generated during assembly draws the complex together, bringing the synaptic vesicle and presynaptic membranes into close proximity and placing the synaptic vesicle in a pre-fusion state. Syt1, the primary Ca^{2+} sensor, located on the vesicle membrane, binds Ca^{2+} to fully zipper the SNARE complex helical bundle, thereby accelerating synaptic vesicle fusion with the presynaptic membrane and neurotransmitter release [64]. Study demonstrated that enhancing Snap25 and Syt1 function promotes synaptic vesicle trafficking in cortical neurons [38]. Thus, synaptic vesicle fusion and release functions require the joint action of the SNARE complex and its chaperone molecules.

Dysfunctional synaptic vesicle fusion and release, mediated by the SNARE complex, are important causes of impaired synaptic function in the DLPFC of AD patients. Transcriptomic profiling of postmortem DLPFC tissues from AD patients revealed significant downregulation of Snap25, STX1A, Syt1, and VAMP2 [65]. Further studies have shown that reduced *SNARE* gene expression in AD brain tissue, inhibiting chaperone protein function and complex formation, directly contributes to cognitive deterioration [24]. Consistent with these previous findings, we demonstrated impaired SNARE complex assembly in the left PFC of early AD model mice, primarily characterized by reductions in the SNARE complex, Snap25, and Syt1. Conversely, tDCS increased the expression of the SNARE complex, Snap25, and Syt1, and elevated intracellular Ca^{2+} concentrations in left PFC neurons. To further investigate the role of the SNARE complex in synaptic vesicle fusion and release, we conducted functional validation experiments. Using established methodologies, we constructed a rAAV to inhibit SNARE expression [66]. We found that inhibiting the SNARE complex in the left PFC blocked the beneficial effects of tDCS on both working memory and synaptic transmission. This blockade may be attributed to the following reasons. First, given that SNARE complex assembly requires STX1A, Snap25, and VAMP2, the reduced availability of VAMP2 likely constrained complex formation. Second, inhibiting the SNARE complex weakened the interaction between Syt1 and Snap25 while enhancing the binding of Munc18-1 to free STX1A. Increased binding of Munc18-1 to free STX1A hindered the latter's incorporation into the SNARE complex. In line with this, the observed downregulation of Munc13-1 impeded the dissociation of Munc18-1 from STX1A, further explaining the reduction in SNARE complex assembly. Together, these results indicate that tDCS promotes synaptic vesicle fusion and release through coordinated regulation of SNARE complexes and their associated chaperone molecules.

This study delineates the effects of tDCS on SNARE-mediated synaptic vesicle fusion and release processes in the left PFC of AD model mice, and reveals the neurobiological mechanisms by which it ameliorates early-stage AD working memory deficits. Nevertheless, our present study has several limitations. First, the 5×FAD murine model recapitulates Aβ pathology and neuronal degeneration but lacks neurofibrillary tangles, a defining tauopathic feature of human AD. Its accelerated amyloidogenesis deviates from human disease progression timelines, while rodent behavioral paradigms incompletely model complex human cognitive deficits. Second, tDCS efficacy may be compromised by current instability, cranial periosteal thickness variability, skin impedance fluctuations, and individual differences in tolerance/nociceptive thresholds. Third, there are certain limitations in the experimental design. Our study only examined Snap25 and Syt1 in the four groups: WT, AD, Sham-tDCS, and tDCS, while lacking detection of STX1A, VAMP2, and the chaperone molecules Munc18-1 and Munc13-1. Additionally, the interaction between VAMP2 and Syt1 was not assessed. In terms of behavioral testing, although both the T-maze and Y-maze are valid methods for evaluating working memory in animals, for greater rigor, the behavioral tests across the three studies should have been consistent. Fourth, the present study focused on the short-term effects of tDCS, but did not explore in depth its sustained impact on working memory and synaptic function. The future study should focus on assessing the long-term effects of tDCS. Fifth, while our

model was supported by functional evidence, it lacked direct ultrastructural validation through synaptic labeling or other visualization techniques [67]. Sixth, the sample sizes for specific experimental techniques in this study were relatively small, which may have limited the statistical power of the analyses. In addition, the working memory network involves not only the left PFC but also synergistic modulation across multiple brain regions, so future consideration should be given to expanding the stimulation strategy to multiple regions for synchronized or sequential stimulation to better understand the mechanism of action of tDCS in ameliorating working memory deficits. Important phylogenetic constraints should be considered. The murine PFC lacks both the granular laminar organization and Brodmann-area differentiation characteristic of the human DLPFC. It remains incapable of supporting higher-order cognitive operations such as abstract reasoning or language. These anatomical and functional disparities invite appropriate humility in cross-species evolutionary comparisons. Thus, while conserved cognitive mechanisms validate the translational potential of our targeting strategy, the observed interspecies differences warrant circumspection when extrapolating mechanistic findings.

Conclusions

tDCS activated the excitability of excitatory neuronal activity and increased the number of presynaptic vesicles by stimulating the left PFC, while SNARE complex formation and its interaction with chaperone molecules promoted the fusion and release of synaptic vesicles, which improved the early working memory capacity of AD mice.

Abbreviations

Aβ: Amyloid β-protein
AD: Alzheimer's disease
AP: Action potentials
APP/PS1: Mo/HuAPP695swe and PS1-dE9
AQP4: Aquaporin-4
CBV: Cerebral blood volume
CO-IP: Co-immunoprecipitation
Cho: Choline
Cr: Creatinine
3D: Three-dimensional
DLPFC: Dorsolateral prefrontal cortex
EEG: Electroencephalogram
EGFP: Enhanced green fluorescent protein
5×FAD: Transgenic mice with 5 familial AD
fEPSP: Field excitatory postsynaptic potential
FOV: Field of view
FUS: Functional ultrasound imaging
FQ: Fast alignment sequence quality
ΔF/F: Fluorescence change values
GAPDH: Glyceraldehyde-3-phosphate dehydrogenase
GO: Gene Ontology
GO_C: Gene Ontology cellular component
GO_F: Gene Ontology molecular function
Glu: Glutamate
^{1}H-MRS: Hydrogen proton magnetic resonance spectroscopy
I/O curves: Input/output curves
KEGG: Kyoto Encyclopedia of Genes and Genomes
LRP1: Low-density lipoprotein receptor-related protein 1
Munc13-1: Mammalian unc-13 homolog A
Munc18-1: Syntaxin-binding protein 1
MWM: Morris water maze
NAA: N-acetylaspartate
NOR: Novel object recognition test
MAPK: Mitogen-activated protein kinase
MRS: Magnetic resonance spectroscopy scanning
Opt: Optogenetic
PBS: Phosphate-buffered saline
PCA: Principal component analysis
PFC: Prefrontal cortex
PPR: Paired-pulse ratio
PRESS: Single-pixel sequence point-resolved spectroscopy
ROI: Region of interest
SLC17A6: Solute carrier family 17 member 6
SLC17A7: Solute carrier family 17 member 7
Snap25: Synaptosomal-associated 25 kD protein
SNARE: Soluble N-ethylmaleimide-sensitive factor attachment receptor
STX1A: Syntaxin 1A
Syt1: Synaptotagmin-1
T2WI: T2-weighted image
tDCS: Transcranial direct current stimulation
TE: Echo time
TEM: Transmission electron microscopy
TF: Exploration times for the familiar
TGF: transforming growth factor
TN: Exploration times for the novel
TR: Repetition time
U-MAP: Uniform manifold approximation and projection
VAMP2: Vesicle associated membrane protein 2
VGLUT1: Vesicular glutamate transporter 1
WT: Wild-type.

Supplementary information

The online version contains supplementary material available at https://doi.org/10.1016/j.mmr.2026.100003.

Additional file 1. Materials and methods. Fig. S1 tDCS stimulation of the left prefrontal cortex (PFC) increased neuronal excitability in 5× FAD mice. **Fig. S2** Soluble N-ethylmaleimide-sensitive factor attachment receptor (SNARE)-inhibitory viruses decreased working memory function in 5× FAD mice.

Acknowledgements

We thank Tingting Jin for her guidance. We also acknowledge the use of Kimi and DeepSeek for polishing the abstract and introduction sections. Additionally, we thank Genesis Technology Communication (Beijing), Co., Ltd. for providing professional language editing services during the preparation of this manuscript.

Authors' contributions

YYZ, JMY, TCW, and WLL contributed to the experimental design. YYZ,

JMY, WSX, BW, XX, WJW, HWL, JWJ, JZW, TJ, LMC, YXQ, ZYH, YHZ, and TY performed experiments, data collection, and data analysis. YYZ, MGY, JFZ, JT, and LDC contributed to the discussion and interpretation. YYZ, WGL, KY, and WLL reviewed and edited the manuscript. All authors read and approved the final manuscript.

Funding

This work was supported by the National "Ten Thousand People Plan" Young Top Talents Program, and the Chinese Society of Rehabilitation Medicine (KFKT-2022-011).

Availability of data and materials

The data and materials supporting the findings of this study are available upon request.

Declarations

Ethics approval and consent to participate

All experimental procedures in mice were performed in compliance with the protocol approved by the Animal Experiment Ethics Committee of Fujian University of Traditional Chinese Medicine (FJTCMIACUC2023131). Animals were housed in the SPF-level laboratory at the Experimental Animal Center, Fujian University of Traditional Chinese Medicine [SYXK(Fujian)2020-0002].

Consent for publication

Not applicable.

Competing interests

The authors declare that they have no competing interests.

Author details

[1]The Institute of Rehabilitation Industry, Fujian University of Traditional Chinese Medicine, Fuzhou 350122, China. [2]National-Local Joint Engineering Research Center of Rehabilitation Medicine Technology, Fujian University of Traditional Chinese Medicine, Fuzhou 350122, China. [3]State Key Laboratory for Quality Ensurance and Sustainable Use of Dao-di Herbs, Artemisinin Research Center, and Institute of Chinese Materia Medica, China Academy of Chinese Medical Sciences, Beijing 100700, China. [4]The State Key Laboratory of Brain and Cognitive Sciences, the University of Hong Kong, Hong Kong SAR 999077, China. [5]Children Hospital of Fudan University, Shanghai 201102, China.

References

1. Scheltens P, De Strooper B, Kivipelto M, Holstege H, Chetelat G, Teunissen CE, *et al*. Alzheimer's disease. Lancet. 2021;397(10284):1577-90.
2. Huntley J, Bor D, Hampshire A, Owen A, Howard R. Working memory task performance and chunking in early Alzheimer's disease. Br J Psychiatry. 2011;198(5):398-403.
3. Couzin-Frankel J. Side effects loom over Alzheimer's drugs. Science. 2023;381(6657):466-7.
4. Hyde J, Carr H, Kelley N, Seneviratne R, Reed C, Parlatini V, *et al*. Efficacy of neurostimulation across mental disorders: systematic review and meta-analysis of 208 randomized controlled trials. Mol Psychiatry. 2022;27(6):2709-19.
5. Yang Y, Cao TQ, He SH, Wang LC, He QH, Fan LZ, *et al*. Revolutionizing treatment for disorders of consciousness: a multidisciplinary review of advancements in deep brain stimulation. Mil Med Res. 2024;11(1):81.
6. Maisson DJ, Gemzik ZM, Griffin AL. Optogenetic suppression of the nucleus reuniens selectively impairs encoding during spatial working memory. Neurobiol Learn Mem. 2018;155:78-85.
7. Chu CS, Li CT, Brunoni AR, Yang FC, Tseng PT, Tu YK, *et al*. Cognitive effects and acceptability of non-invasive brain stimulation on Alzheimer's disease and mild cognitive impairment: a component network meta-analysis. J Neurol Neurosurg Psychiatry. 2021;92(2):195-203.
8. Duan M, Meng Z, Yuan D, Zhang Y, Tang T, Chen Z, *et al*. Anodal and cathodal transcranial direct current stimulations of prefrontal cortex in a rodent model of Alzheimer's disease. Front Aging Neurosci. 2022;14:968451.
9. Cespón J, Rodella C, Miniussi C, Pellicciari MC. Behavioural and electrophysiological modulations induced by transcranial direct current stimulation in healthy elderly and Alzheimer's disease patients: a pilot study. Clin Neurophysiol. 2019;130(11):2038-52.
10. Satorres E, Escudero Torrella J, Real E, Pitarque A, Delhom I, Melendez JC. Home-based transcranial direct current stimulation in mild neurocognitive disorder due to possible Alzheimer's disease. A randomised, single-blind, controlled-placebo study. Front Psychol. 2022;13:1071737.
11. Barbati SA, Podda MV, Grassi C. Tuning brain networks: The emerging role of transcranial direct current stimulation on structural plasticity. Front Cell Neurosci. 2022;16:945777.
12. Wang Y, Wang J, Zhang QF, Xiao KW, Wang L, Yu QP, *et al*. Neural mechanism underlying task-specific enhancement of motor learning by concurrent transcranial direct current stimulation. Neurosci Bull. 2023;39(1):69-82.
13. Yan Z, Rein B. Mechanisms of synaptic transmission dysregulation in the prefrontal cortex: pathophysiological implications. Mol Psychiatry. 2022;27(1):445-65.
14. Owen AM. The functional organization of working memory processes within human lateral frontal cortex: the contribution of functional neuroimaging. Eur J Neurosci. 1997;9(7):1329-39.
15. Li H, Mclaurin KA, Mactutus CF, Likins B, Huang W, Chang SL, *et al*. Intraneuronal β-amyloid accumulation: aging HIV-1 human and HIV-1 transgenic rat brain. Viruses. 2022;14(6):1268.
16. Kumar S, Zomorrodi R, Ghazala Z, Goodman MS, Blumberger DM, Daskalakis ZJ, *et al*. Effects of repetitive paired associative stimulation on brain plasticity and working memory in Alzheimer's disease: a pilot randomized double-blind-controlled trial. Int Psychogeriatr. 2023;35(3):143-55.
17. Evangelista ND, O'shea A, Kraft JN, Hausman HK, Boutzoukas EM, Nissim NR, *et al*. Independent contributions of dorsolateral prefrontal structure and function to working memory in healthy older adults. Cereb Cortex. 2021;31(3):1732-43.
18. Kumar S, Zomorrodi R, Ghazala Z, Goodman MS, Blumberger DM, Cheam A, *et al*. Extent of dorsolateral prefrontal cortex plasticity and its association with working memory in patients with alzheimer disease. JAMA Psychiatry. 2017;74(12):1266-74.
19. Hansel D, Mato G. Short-term plasticity explains irregular persistent activity in working memory tasks. J Neurosci. 2013;33(1):133-49.
20. Südhof TC, Rothman JE. Membrane fusion: grappling with SNARE and SM proteins. Science. 2009;323(5913):474-7.
21. Kandimalla R, Reddy PH. Therapeutics of neurotransmitters in Alzheimer's disease. J Alzheimers Dis. 2017;57(4):1049-69.
22. Wang YN, Figueiredo D, Sun XD, Dong ZQ, Chen WB, Cui WP, *et al*.

Controlling of glutamate release by neuregulin3 via inhibiting the assembly of the SNARE complex. Proc Natl Acad Sci U S A. 2018;115(10):2508-13.
23. Eriksen J, Li F, Edwards RH. The mechanism and regulation of vesicular glutamate transport: Coordination with the synaptic vesicle cycle. Biochim Biophys Acta Biomembr. 2020;1862(12): 183259.
24. Williams JB, Cao Q, Yan Z. Transcriptomic analysis of human brains with Alzheimer's disease reveals the altered expression of synaptic genes linked to cognitive deficits. Brain Commun. 2021;3(3):fcab123.
25. Bao H, Das D, Courtney NA, Jiang Y, Briguglio JS, Lou X, *et al*. Dynamics and number of trans-SNARE complexes determine nascent fusion pore properties. Nature. 2018;554(7691):260-3.
26. Hu S, Wang H, Chen K, Cheng P, Gao S, Liu J, *et al*. MicroRNA-34c downregulation ameliorates amyloid-β-induced synaptic failure and memory deficits by targeting VAMP2. J Alzheimers Dis. 2015;48(3):673-86.
27. Chen XQ, Zuo X, Becker A, Head E, Mobley WC. Reduced synaptic proteins and SNARE complexes in Down syndrome with Alzheimer's disease and the Dp16 mouse Down syndrome model: Impact of APP gene dose. Alzheimers Dement. 2023;19(5):2095-116.
28. Podda MV, Cocco S, Mastrodonato A, Fusco S, Leone L, Barbati SA, *et al*. Anodal transcranial direct current stimulation boosts synaptic plasticity and memory in mice via epigenetic regulation of Bdnf expression. Sci Rep. 2016;6:22180.
29. Vasu SO, Kaphzan H. The role of axonal voltage-gated potassium channels in tDCS. Brain Stimul. 2022;15(3):861-9.
30. Barbati SA, Cocco S, Longo V, Spinelli M, Gironi K, Mattera A, *et al*. Enhancing plasticity mechanisms in the mouse motor cortex by anodal transcranial direct-current stimulation: the contribution of nitric oxide signaling. Cereb Cortex. 2020;30(5):2972-85.
31. Wang KW, Ye XL, Huang T, Yang XF, Zou LY. Optogenetics-induced activation of glutamate receptors improves memory function in mice with Alzheimer's disease. Neural Regen Res. 2019; 14(12):2147-55.
32. Cai G, Lu Y, Chen J, Yang D, Yan R, Ren M, *et al*. Brain-wide mapping of c-Fos expression with fluorescence micro-optical sectioning tomography in a chronic sleep deprivation mouse model. Neurobiol Stress. 2022;20:100478.
33. Long JM, Holtzman DM. Alzheimer disease: an update on pathobiology and treatment strategies. Cell. 2019;179(2):312-39.
34. Carvalho TP, Buonomano DV. Differential effects of excitatory and inhibitory plasticity on synaptically driven neuronal input-output functions. Neuron. 2009;61(5):774-85.
35. Dai Y, Zhang Y, Yang M, Lin H, Liu Y, Xu W, *et al*. Electroacupuncture Increases the hippocampal synaptic transmission efficiency and long-term plasticity to improve vascular cognitive impairment. Mediators Inflamm. 2022;2022:5985143.
36. Goossens J, Cervantes Gonzalez A, Dewit N, Lidon L, Fortea J, Alcolea D, *et al*. Evaluation of cerebrospinal fluid levels of synaptic vesicle protein, VAMP-2, across the sporadic Alzheimer's disease continuum. Alzheimers Res Ther. 2023;15(1):186.
37. Acuna C, Guo Q, Burre J, Sharma M, Sun J, Sudhof TC. Microsecond dissection of neurotransmitter release: SNARE-complex assembly dictates speed and Ca^{2+} sensitivity. Neuron. 2014;82(5):1088-100.
38. Shvarts-Serebro I, Sheinin A, Gottfried I, Adler L, Schottlender N, Ashery U, *et al*. miR-128 as a regulator of synaptic properties in 5xFAD mice hippocampal neurons. J Mol Neurosci. 2021;71(12): 2593-607.
39. Dawidowski D, Cafiso DS. Munc18-1 and the Syntaxin-1 N terminus regulate open-closed states in a t-SNARE complex. Structure. 2016;24(3):392-400.
40. Gilardone G, Longo C, Papagno C. The role of working memory and short-term memory in sentence comprehension: a systematic review and meta-analysis in probable Alzheimer's disease. Neuropsychol Rev. 2024;34(2):530-47.
41. Ruan N, Li X, Xu T, Zhao Z, Mei X, Zheng C. Cortical activation in elderly patients with Alzheimer's disease dementia during working memory tasks: a multichannel fNIRS study. Front Aging Neurosci. 2024;16:1433551.
42. Gagnon LG, Belleville S. Working memory in mild cognitive impairment and Alzheimer's disease: contribution of forgetting and predictive value of complex span tasks. Neuropsychology. 2011;25(2):226-36.
43. Stevens LM, Brown RE. Reference and working memory deficits in the 3xTg-AD mouse between 2 and 15-months of age: a cross-sectional study. Behav Brain Res. 2015;278:496-505.
44. Kosel F, Pelley JMS, Franklin TB. Behavioural and psychological symptoms of dementia in mouse models of Alzheimer's disease-related pathology. Neurosci Biobehav Rev. 2020;112:634-47.
45. Webler RD, Fox J, Mcteague LM, Burton PC, Dowdle L, Short EB, *et al*. DLPFC stimulation alters working memory related activations and performance: an interleaved TMS-fMRI study. Brain Stimul. 2022;15(3):823-32.
46. Goldthorpe RA, Rapley JM, Violante IR. A Systematic review of non-invasive brain stimulation applications to memory in healthy aging. Front Neurol. 2020;11:575075.
47. Stavroulaki V, Ioakeimidis V, Konstantoudaki X, Sidiropoulou K. Enhanced synaptic properties of the prefrontal cortex and hippocampus after learning a spatial working memory task in adult male mice. J Neurosci Res. 2021;99(7):1802-14.
48. Okur Z, Schlauri N, Bitsikas V, Panopoulou M, Ortiz R, Schwaiger M, *et al*. Control of neuronal excitation-inhibition balance by BMP-SMAD1 signalling. Nature. 2024;629(8011):402-9.
49. Berglund K, Stern MA, Gross RE. Bioluminescence-optogenetics. Adv Exp Med Biol. 2021;1293:281-93.
50. Cardoso-Cruz H, Paiva P, Monteiro C, Galhardo V. Selective optogenetic inhibition of medial prefrontal glutamatergic neurons reverses working memory deficits induced by neuropathic pain. Pain. 2019;160(4):805-23.
51. Kim S, Chun H, Kim Y, Kim Y, Park U, Chu J, *et al*. Astrocytic autophagy plasticity modulates Abeta clearance and cognitive function in Alzheimer's disease. Mol Neurodegener. 2024;19(1):55.
52. Tarasoff-Conway JM, Carare RO, Osorio RS, Glodzik L, Butler T, Fieremans E, *et al*. Clearance systems in the brain-implications for Alzheimer disease. Nat Rev Neurol. 2015;11(8):457-70.
53. Simon M, Wang MX, Ismail O, Braun M, Schindler AG, Reemmer J, *et al*. Loss of perivascular aquaporin-4 localization impairs glymphatic exchange and promotes amyloid beta plaque formation in mice. Alzheimers Res Ther. 2022;14(1):59.
54. Kavalali ET, Jorgensen EM. Visualizing presynaptic function. Nat Neurosci. 2014;17(1):10-6.
55. Cottrell JR, Levenson JM, Kim SH, Gibson HE, Richardson KA, Sivula M, *et al*. Working memory impairment in calcineurin knock-out mice is associated with alterations in synaptic vesicle cycling and disruption of high-frequency synaptic and network activity in prefrontal cortex. J Neurosci. 2013;33(27):10938-49.
56. Walker CK, Herskowitz JH. Dendritic spines: mediators of cognitive

resilience in aging and Alzheimer's disease. Neuroscientist. 2021;27(5):487-505.
57. Chakroborty S, Hill ES, Christian DT, Helfrich R, Riley S, Schneider C, *et al*. Reduced presynaptic vesicle stores mediate cellular and network plasticity defects in an early-stage mouse model of Alzheimer's disease. Mol Neurodegener. 2019;14(1):7.
58. Yuan Y, Li Y, Yang F, Jiang Y, Ding Y, Xiao Y, *et al*. Sh3rf3 deficiency drives autism-like behaviors via presynaptic dysfunction in mice. Mol Psychiatry. 2025; doi: 10.1038/s41380-025-03370-w.
59. Urbina FL, Gupton SL. SNARE-mediated exocytosis in neuronal development. Front Mol Neurosci. 2020;13:133.
60. Sudhof TC. The molecular machinery of neurotransmitter release (Nobel lecture). Angew Chem Int Ed Engl. 2014;53(47):12696-717.
61. Wang X, Gong J, Zhu L, Wang S, Yang X, Xu Y, *et al*. Munc13 activates the Munc18-1/syntaxin-1 complex and enables Munc18-1 to prime SNARE assembly. Embo J. 2020;39(16):e103631.
62. Wang S, Li Y, Gong J, Ye S, Yang X, Zhang R, *et al*. Munc18 and Munc13 serve as a functional template to orchestrate neuronal SNARE complex assembly. Nat Commun. 2019;10(1):69.
63. Jiao J, Rebane AA, Ma L, Zhang Y. Single-molecule protein folding experiments using high-precision optical tweezers. Methods Mol Biol. 2017;1486:357-90.
64. Rizo J. Mechanism of neurotransmitter release coming into focus. Protein Sci. 2018;27(8):1364-91.
65. Ochneva A, Zorkina Y, Abramova O, Pavlova O, Ushakova V, Morozova A, *et al*. Protein misfolding and aggregation in the brain: common pathogenetic pathways in neurodegenerative and mental disorders. Int J Mol Sci. 2022;23(22):14498.
66. Huang X, Huang P, Huang L, Hu Z, Liu X, Shen J, *et al*. A visual circuit related to the nucleus reuniens for the spatial-memory-promoting effects of light treatment. Neuron. 2021;109(2):347-62.e7.
67. Zhao Y, Cheng L, Xu R, Yu Z, Zhang J. Research progress and applications of optoelectronic synaptic devices based on 2D materials. Brain-X. 2024;2(3):e70004.

https://doi.org/10.1016/j.mmr.2026.100003
Cite this article as: Zhuang YY, Yan JM, Wu TC, Xu WS, Wu B, Xie X, *et al*. tDCS improves early Alzheimer's disease by synaptic vesicle fusion and release. *Mil Med Res*. 2026;13(1):100003.